Copyright Warning & Restrictions

The copyright law of the United States (Title 17, United States Code) governs the making of photocopies or other reproductions of copyrighted material.

Under certain conditions specified in the law, libraries and archives are authorized to furnish a photocopy or other reproduction. One of these specified conditions is that the photocopy or reproduction is not to be "used for any purpose other than private study, scholarship, or research." If a, user makes a request for, or later uses, a photocopy or reproduction for purposes in excess of "fair use" that user may be liable for copyright infringement,

This institution reserves the right to refuse to accept a copying order if, in its judgment, fulfillment of the order would involve violation of copyright law.

Please Note: The author retains the copyright while the New Jersey Institute of Technology reserves the right to distribute this thesis or dissertation

Printing note: If you do not wish to print this page, then select "Pages from: first page # to: last page #" on the print dialog screen

ABSTRACT

IMPAIRMENTS IN GROUND MOVING TARGET INDICATOR (GMTI) RADAR

by
Phuoc Doan Huu Vu

Radars on multiple distributed airborne or ground based moving platforms are of increasing interest, since they can be deployed in close proximity to the event under investigation and thus offer remarkable sensing opportunities. Ground moving target indicator (GMTI) detects and localizes moving targets in the presence of ground clutter and other interference sources. Space-time adaptive processing (STAP) implemented with antenna arrays has been a classical approach to clutter cancellation in airborne radar. One of the challenges with STAP is that the minimum detectable velocity (MDV) of targets is a function of the baseline of the antenna array: the larger the baseline (i.e., the narrower the beam), the lower the MDV. Unfortunately, increasing the baseline of a uniform linear array (ULA) entails a commensurate increase in the number of elements. An alternative approach to increasing the resolution of a radar, is to use a large, but sparse, random array. The proliferation of relatively inexpensive autonomous sensing vehicles, such as unmanned airborne systems, raises the question whether is it possible to carry out GMTI by distributed airborne platforms. A major obstacle to implementing distributed GMTI is the synchronization of autonomous moving sensors. For range processing, GMTI processing relies on synchronized sampling of the signals received at the array, while STAP processing requires time, frequency and phase synchronization for beamforming and interference cancellation. Distributed sensors have independent oscillators, which are naturally not synchronized and are each subject to different stochastic phase drift. Each sensor has its own local oscillator, unlike a traditional array in which all sensors are connected to the same local oscillator. Even when

tuned to the same frequency, phase errors between the sensors will develop over time, due to phase instabilities. These phase errors affect a distributed STAP system. In this dissertation, a distributed STAP application in which sensors are moving autonomously is envisioned. The problems of tracking, detection for our proposed architecture are of important.

The first part focuses on developing a direct tracking approach to multiple targets by distributed radar sensors. A challenging scenario of a distributed multi-input multi-output (MIMO) radar system (as shown above), in which relatively simple moving sensors send observations to a fusion center where most of the baseband processing is performed, is presented. The sensors are assumed to maintain time synchronization, but are not phase synchronized. The conventional approach to localization by distributed sensors is to estimate intermediate parameters from the received signals, for example time delay or the angle of arrival. Subsequently, these parameters are used to deduce the location and velocity of the target(s). These classical localization techniques are referred to as indirect localization. Recently, new techniques have been developed capable of estimating target location directly from signal measurements, without an intermediate estimation step. The objective is to develop a direct tracking algorithm for multiple moving targets. It is aimed to develop a direct tracking algorithm of targets state parameters using widely distributed moving sensors for multiple moving targets. Potential candidate for the tracker include Extended Kalman Filter.

In the second part of the dissertation,the effect of phase noise on space-time adaptive processing in general, and spatial processing in particular is studied. A power law model is assumed for the phase noise. It is shown that a composite model with several terms is required to properly model the phase noise. It is further shown that the phase noise has almost linear trajectories. The effect of phase noise on spatial processing is analyzed. Simulation results illustrate the

effect of phase noise on degrading the performance in terms of beampattern and receiver operating characteristics. A STAP application, in which spatial processing is performed (together with Doppler processing) over a coherent processing interval, is envisioned.

IMPAIRMENTS IN GROUND MOVING TARGET INDICATOR (GMTI) RADAR

by
Phuoc Doan Huu Vu

A Dissertation
Submitted to the Faculty of
New Jersey Institute of Technology
in Partial Fulfillment of the Requirements for the Degree of
Doctor of Philosophy in Electrical Engineering

Helen and John C. Hartmann
Department of Electrical and Computer Engineering

December 2018

APPROVAL PAGE

IMPAIRMENTS IN GROUND MOVING TARGET INDICATOR (GMTI) RADAR

Phuoc Doan Huu Vu

Dr. Alexander M. Haimovich, Dissertation Advisor — Date
Distinguished Professor of Electrical and Computer Engineering, NJIT

Dr. Osvaldo Simeone, Committee Member — Date
Professor of Information Engineering, King's College London

Dr. Joerg Kliewer, Committee Member — Date
Professor of Electrical and Computer Engineering, NJIT

Dr. Ali Abdi, Committee Member — Date
Professor of Electrical and Computer Engineering, NJIT

Dr. Braham Himed, Committee Member — Date
RF Technology Branch, Air Force Research Lab (AFRL/RYMD)

BIOGRAPHICAL SKETCH

Author: Phuoc Doan Huu Vu

Degree: Doctor of Philosophy

Date: December 2018

Undergraduate and Graduate Education:

- Doctor of Philosophy in Electrical Engineering,
  New Jersey Institute of Technology, Newark, NJ, 2018
- Master of Science in Electrical Engineering,
  Louisiana State University, Baton Rouge, LA 2014
- Bachelor of Science in Electrical Engineering,
  Louisiana Tech University, Ruston, LA 2012

Major: Electrical Engineering

Presentations and Publications:

Phuoc Vu, Alexander M. Haimovich and Braham Himed, "Effects of System Impairments on the Performance of Distributed STAP," To be submitted to *IEEE Radar Conference 2019*.

Phuoc Vu, Alexander M. Haimovich and Braham Himed, "Effect of Phase Noise and Other Impairments on Distributed STAP," To be submitted to *IEEE Trans. on Aerospace and Electron. Syst.*

Phuoc Vu, Alexander M. Haimovich and Braham Himed, "Effect of Phase Noise on Spatial Processing by Sensors with Independent Oscillators," in *Proc. IEEE Radar Conf.*, pp. 1-6, May 2018.

Phuoc Vu, Alexander M. Haimovich and Braham Himed, "Bayesian Cramer-Rao Bound for Multiple Targets Tracking in MIMO Radar," in *Proc. IEEE Radar Conf.*, pp. 980-985, May 2017.

Phuoc Vu, Alexander M. Haimovich and Braham Himed, "Direct Tracking of Multiple Targets in MIMO Radar," in *2016 50th Asilomar Conference on Signals, Systems and Computers, Pacific Grove, CA*, pp. 1139-1143, November 2016.

To my parents who taught me compassion, hardwork and perseverance.
To my parents-in-law who taught me that selfless acts of kindness matter the most.
To my beloved wife who make my life complete in every sense.

ACKNOWLEDGMENT

First and foremost, I would like to express my sincerest gratitude to my dissertation advisor, Professor Alexander M. Haimovich for the opportunity to pursue my PhD degree, funding my research, his invaluable and insightful guidance throughout the course of my PhD study. I am so grateful for his kind support and guidance that helped me to succeed in my research career and grow as an engineer. He gave me the main idea of this work, and without his continuous encouragement next to his deep knowledge of communication, this dissertation could not have been accomplished. I learned from him how to scientifically approach problems and develop the true spirit of a diligent researcher.

I would also like to express my gratitude to Professors Osvaldo Simeone, Ali Abdi, and Joerg Kliewer as well as Dr. Braham Himed for serving as my committee members. I personally would like to thank Dr. Braham Himed for the funding I received during my PhD studies and for sharing his deep technical knowledge through his advices and recommendations of my research.

I also want to thank all my colleagues at NJIT, who went on this academic journey with me. In particular, I'd like to thank Haley, Wei, Annan, Kyle. I'd also like to thank Angela Retino and Kathy Bosco for their friendship over the years and their help with all the administrative matters during my PhD studies.

Lastly, I want to thank my fathers, Hoc Vu and Hanh Nguyen, my mothers, Thanh Doan and Tuyet Doan, my late brother, Hieu Vu, and my wife, Hoa Nguyen, for their constant support and understanding. I am especially indebted to my wife who have gone through this long journey with me.

TABLE OF CONTENTS

TABLE OF CONTENTS
(Continued)

Chapter **Page**

LIST OF TABLES

Table **Page**

LIST OF FIGURES

LIST OF FIGURES
(Continued)

Figure **Page**

CHAPTER 1

INTRODUCTION

Detection, localization and tracking of ground moving targets are key radar functions that contribute to continued U.S. warfighting dominance. Radars on multiple distributed airborne or ground based moving platforms are of increasing interest, since they can be deployed in close proximity to the event under investigation and thus offer remarkable sensing opportunities [1]. For example, unmanned aerial vehicles (UAVs) based radars play a significant role in disaster relief efforts by quickly flying to the impacted area and providing the most accurate and updated information [2]. In urban sensing environments, potential targets may be obscured by buildings and other man-made structures; with sensors on moving platforms, the subject area can be probed from more favorable positions to yield enhanced detectability [3]. Other applications of radar on moving platforms for military and civilian sensing operations can be found in, e.g., [4], [5], [6].

Ground moving target indication (GMTI) radar [7]–[11] is an airborne radar tasked with detecting the presence of moving targets in an environment where the interference due to ground clutter can be severe. GMTI radars therefore is expected to be able to perform target detection while suppressing the interference due to ground clutter. The ground clutter as seen by the airborne radar, exists at every angle, in addition, due to the platform velocity of the aircraft, the ground clutter also exists for all Dopplers. To take advantage of the structure of the clutter ridge, researchers have considered space-time adaptive processing (STAP) [12]–[14], which performs joint processing in both spatial and temporal domains simultaneously. Since the clutter does not occupy the entire angle-Doppler map, separating the target from the clutter

is possible with STAP, assuming that the target is sufficiently far from the clutter ridge on the angle-Doppler map.

The proliferation of airborne, inexpensive radio frequency sensors recently raises interest in distributed implementation of radar systems. Figure 1.1 shows the two design aspects of distributed radar systems. While STAP methods have improved over

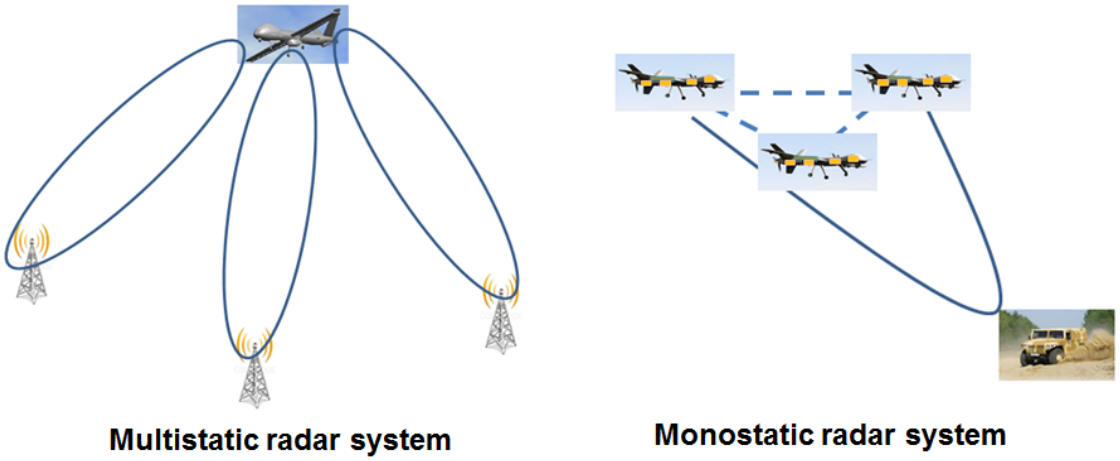

Figure 1.1 Distributed Radar Architectures.

the years, including the latest developments reported above, STAP relies on a carefully calibrated phased array, which implies a highly specialized plat- form dedicated to the GMTI task. Moreover, the performance of STAP depends on the array baseline, which is ultimately limited by the size of the platform. In this dissertation, we proposed an approach radically different than STAP, in which sensors are assumed to maintain global time synchronization (e.g., through GPS), but are not phase synchronized. For example, the method would be suitable for implementation by widely distributed, independently moving UAVs, each with its own free-running local oscillator. To support Doppler processing, the oscillator at each sensor is assumed to maintain coherency over the observation time interval, but unlike a phased array, local oscillators are not phase synchronized to each other. To distinguish it from conventional STAP, we refer to this method as distributed STAP. With a system

that consists of simple, opportunistic sensors, the processing load is shifted to a fusion center equipped with powerful processing capabilities. Figure 1.2 shows the proposed distributed STAP architecture. Target detection and localization are only

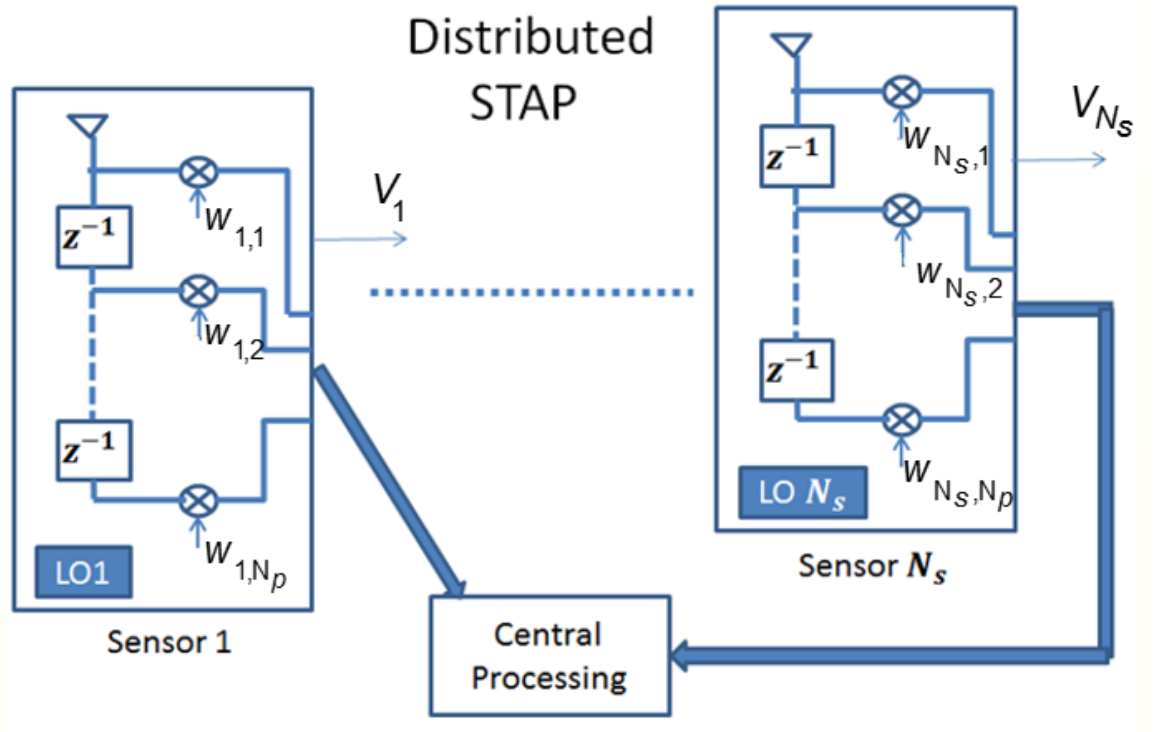

Figure 1.2 Distributed STAP Architectures.

part of the functions required to achieve full situational awareness. There are several challenges posed for a distributed STAP radar system. First, forming tracks and target tracking using distributed sensors are important functions of radar and inquired more understandings. Second, distributed sensors are impacted by independent phase noise. Third, time and phase synchronization of distributed, airborne platforms need to be carefully analyzed. Last, but not least, target detection from measurements by distributed, moving platforms spaced irregularly at more than half-wavelength should also be studied. In this dissertation, we look into certain aspects of a distributed implementation of STAP and address each challenging aspects mentioned above.

1.1 Direct Tracking of Multiple Targets in Distributed MIMO Radar System

The conventional approach to localization by distributed sensors is to use signal observations to first estimate parameters, such as time delay or the angle of incidence of the wave, and subsequently apply these estimates to deduce the location and velocity of targets. Since they rely on estimating intermediate parameters, classical localization techniques may be referred to as indirect localization. Recently, new techniques capable of estimating target location directly from signal measurements without an intermediate estimation step have been developed. It is shown that in some conditions, such techniques may provide significantly better performance [15]. Direct localization has been applied to Doppler estimation [16], to multiple input multiple output (MIMO) radar [16], localization in multipath [17], and to tracking of single targets [16].

When a target is in motion, the localization problem becomes a tracking problem. The Kalman filter is a classical tracking algorithm applied to a state space model that consists of a kinematic model and an observation model. The Kalman algorithm estimates the state of a process in a way that minimizes the estimation mean square error (MSE) [4], [5]. The extended Kalman filter is a variation of the Kalman filter that may be applied when the observation model is non-linear in the state parameters. In [6], a tracker based on the extended Kalman filter in a widely-distributed MIMO radar setting, was developed for a single target. Each sensor estimates the targets location and velocity locally, and sends the estimates to a central fusion center, where the track is formed and maintained.

In contrast to the literature reviewed above, in this work, we are interested in multiple targets tracking (MTT). MTT is a well known problem with a rich literature [7-13], [18]. Given a varying number of targets as a function of time, with new targets joining in and others dropping out, the purpose of multi-target tracking is to

associate measurements with the targets that have generated them [19]. A primary task of an MTT system is data association, i.e., partitioning the measurements into disjoint sets, each set generated from a single target. The data association problem may be formulated in several ways. For example, measurements may be classified into tracks by determining the nearest neighbor observation to an existing track. Other approaches seek to avoid the explicit data association step by generalizing the state vector to incorporate multiple targets [20]. In Chapter 2, we propose a tracker based on the extended Kalman filter that tracks multiple targets based on an observation model in which radar observations are non-linear functions of the targets' states. We refer to this tracker as direct, since it achieves tracking directly from radar observations, rather than from time delays and Doppler shifts. It is noted that a direct tracker based on a particle filter was proposed in [16], but that tracker was limited to a single target.

Furthermore, we proposed new tracking algorithms and performance bounds for multiple targets in non-coherent, multistatic MIMO radar. Specific contributions are: (1) extension of a MIMO radar indirect tracking scheme originally proposed in [21] for single target to two targets, by incorporating nearest neighbor data association; (2) a new Kalman filter direct tracking scheme for multiple targets, in which tracks are formed and maintained at a fusion center from observations communicated by sensors of a MIMO radar.

1.2 Effect of Phase Noise and Other Impairments on Distributed STAP

Radars on multiple distributed airborne or ground based moving platforms are of increasing interest, since they can be deployed in close proximity to the event under investigation and thus offer remarkable sensing opportunities [1]. For example, unmanned aerial vehicles (UAVs) based radars play a significant role in disaster relief efforts by quickly flying to the impacted area and providing the most accurate

and updated information [2]. In urban sensing environments, potential targets may be obscured by buildings and other man-made structures; with sensors on moving platforms, the subject area can be probed from more favorable positions to yield enhanced detectability [3]. Other applications of radar on moving platforms for military and civilian sensing operations can be found in, e.g., [4], [5], [6].

In ground moving target indicator (GMTI), of interest is to determine the presence of targets and their ranges, azimuth angles, and Doppler shifts. Space-time adaptive processing (STAP) enables GMTI radars to perform moving target detection in the presence of ground clutter. STAP implemented with antenna arrays has been a classical approach to clutter cancellation in airborne radar [22, 23]. The proliferation of airborne, inexpensive radio frequency sensors raises interest in distributed implementation of radar systems. In this work, we consider certain aspects of a distributed implementation of STAP.

The power spectral density (PSD) of an ideal sinusoidal carrier observed over $t \to \infty$ is an impulse at f_0. However, practical oscillators have amplitude and phase deviations from the ideal oscillator that cause spreading of the spectrum. The phase deviation of a practical oscillator from the nominal phase $2\pi f_0 t$, where f_0 is the carrier frequency is known as phase noise. The study of phase noise has started more than 50 years ago, as reviewed in a recent retrospective [24]. As explained in [24], diverse applications of oscillators led to a variety of analysis approaches. The lack of a unified approach and the difficulty of the topic resulted in a large number of publications, including in the IEEE Proceedings (for example [25, 26, 27, 28], to name a few). Efforts to consolidate and standardize terms yielded an IEEE standard [29] and a National Institute of Standards publication [30].

The characterization and the effects of phase noise on performance have been topics of interest also to the radar community. Phase deviations accumulate over time, hence the effect of phase noise becomes more pronounced over longer observation

times. It is not surprising then that a significant body of literature addresses the effect of phase noise on synthetic aperture radar (SAR) [31]-[32]. SAR integration times are long and phase noise may have great effect on performance. Although the observation time is not quite as long as in SAR, Doppler processing may also be affected by phase noise, with publications spanning many years from [33] to [34]. In contrast, literature on the effect of phase noise on antenna arrays is difficult to come by for the simple reason that spatial processing relies on differential phase measurements between array elements. When the same oscillator drives all elements, phase noise effects are canceled. However, in a distributed application, different sensors are driven by different oscillators. Different oscillators develop different phase noise characteristics as a function of time, making the array subject to the effect of phase noise errors. Thus, at a given sensor, the phase noise associated with the sensor's oscillator affects Doppler processing, whereas the phase noise between oscillators at different sensors affects spatial processing.

Besides phase noise, a distributed STAP system is also subject to other impairments such as frequency offset, non-uniform motion characteristics of individual sensors, non-uniform and potentially large spacing between array elements, and sensors locations uncertainties, to name a few. Frequency offsets inevitably arise even when all sensors are instructed to tune to the same frequency. Whereas a Doppler shift is caused by relative motion, a carrier frequency offset is caused by the carrier frequency mismatch between transmitter and receiver. A distributed STAP system is subject to errors from carrier frequency offsets (CFO). In [35], the authors investigate the effect of CFO on Doppler centroid estimation in Synthetic Aperture Radar (SAR) and on Direction-Of-Arrival (DOA) estimation in array processing. To the best of our knowledge, there is no past work done on the effect of frequency offset for distributed STAP system.

In addition to frequency offset due to different transmitters and receivers in a distributed system, different sensors move autonomously, and thus may have different velocities and direction of motion. This, in turn, leads to Doppler characteristics that vary among sensors. As a result, space-time steering vectors may not be expressed simply by a Kronecker product, as in traditional STAP. In this work, we analyze the generalized motion of target and sensors in a multistatic setup and highlight the effects of platform motion on the clutter problem. Further, classical STAP is typically implemented with uniform linear arrays (ULA), half-wavelength spacing. A distributed implementation leads to non-uniform and potentially much larger spacings between the array elements. Finally, a rigid implementation on a single platform enables to accurately measure the locations of the array's elements. In a distributed implementation, sensors relative locations vary over time, and any sensor localization method (e.g., GPS) is subject to errors. Relevant to analysis of the effect of element errors in a distributed array, is the analysis of the effect of element errors in arrays with colocated elements [36]). In [37], Flanagan achieved array self-calibration with large sensor position errors. Other papers, for example [38], derived the Cramer-Rao lower bounds of the DOA estimation and array calibration precisions in the case of determined and unknown signals based on the assumptions of small array perturbations.

1.3 Motivation of the Dissertation

This dissertation focuses on certain aspects of a distributed implementation of STAP and to the best of our knowledge address the challenges posed for a distributed STAP radar system. We envisioned a STAP application, in which spatial and Doppler processing are performed over a coherent processing interval.

The contributions of this dissertation are the following:

1. Propose a tracker based on the extended Kalman filter that tracks multiple targets based on an observation model in which radar observations are non-linear functions of the targets' states.

2. Propose new tracking algorithms and performance bounds for multiple targets in non-coherent, multistatic MIMO radar. For this tracker, a new Kalman filter direct tracking scheme for multiple targets is developed, in which tracks are formed and maintained at a fusion center from observations communicated by sensors of a MIMO radar.

3. Demonstrate that a power law phase noise PSD model is suitable for analyzing the distributed radar system.

4. Propose a simplified time-domain model for the phase noise.

5. Develop analytical expressions that quantify the effect of phase noise on the array beampattern as a function of time.

6. Propose a generalized motion model for distributed STAP system.

7. Demonstrate the effect of phase noise and other impairments on target detection by numerical examples of receiver operating characteristics (ROC).

This dissertation is organized as follows: Chapter 2 presents the direct tracking algorithms and performance bounds for multiple targets in distributed MIMO radar system. In Chapter 3, a generalized motion model for distributed STAP system is proposed and the effect of phase noise on distributed STAP system is demonstrated. In Chapter 4, numerical results to demonstrate the effect of other impairments pertaining to a distributed STAP system is shown. In Chapter 6 conclusions are made.

The following notation will be used: boldface is used for matrices (uppercase) and vectors (lowercase); $\|\mathbf{y}\|_p$ denotes p-norm; $(\cdot)^T$ is the transpose operator, $(\cdot)^*$

is complex conjugate and $(\cdot)^H$ is the complex conjugate transpose operator; given a set S, and a matrix $\mathbf{A}$, $|S|$ denotes the cardinality of the set, $\mathbf{A}_S$ is the sub-matrix obtained by the columns of $\mathbf{A}$ indexed in S; similarly, if $\mathbf{x}$ is a vector, the vector $\mathbf{x}_S$ consists of the components of $\mathbf{x}$ indexed by S; $\otimes$ marks the Kronecker product ; $\mathbb{E}[\cdot]$ denotes the expectation operator; $\sim CN(\mathbf{m}, \mathbf{R})$ indicates the complex-valued multivariate Gaussian distribution with mean $\mathbf{m}$ and covariance matrix $\mathbf{R}$.

CHAPTER 2

DIRECT TRACKING OF MULTIPLE TARGETS IN MIMO RADAR

2.1 Introduction

The conventional approach to localization by distributed sensors is to use signal observations to first estimate parameters, such as time delay or the angle of incidence of the wave, and subsequently apply these estimates to deduce the location and velocity of targets. Since they rely on estimating intermediate parameters, classical localization techniques may be referred to as indirect localization. Recently, new techniques capable of estimating target location directly from signal measurements without an intermediate estimation step have been developed. It is shown that in some conditions, such techniques may provide significantly better performance [15]. Direct localization has been applied to Doppler estimation [16], to multiple input multiple output (MIMO) radar [16], localization in multipath [17], and to tracking of single targets [16].

In this work, we are interested in multiple targets tracking (MTT). MTT is a well known problem with a rich literature [7-13], [18]. Given a varying number of targets as a function of time, with new targets joining in and others dropping out, the purpose of multi-target tracking is to associate measurements with the targets that have generated them [19]. A primary task of an MTT system is data association, i.e., partitioning the measurements into disjoint sets, each set generated from a single target. The data association problem may be formulated in several ways. For example, measurements may be classified into tracks by determining the nearest neighbor observation to an existing track. Other approaches seek to avoid the explicit data association step by generalizing the state vector to incorporate multiple targets [20]. In this paper, we propose a tracker based on the extended Kalman filter that

tracks multiple targets based on an observation model in which radar observations are non-linear functions of the targets' states. We refer to this tracker as direct, since it achieves tracking directly from radar observations, rather than from time delays and Doppler shifts. It is noted that a direct tracker based on a particle filter was proposed in [16], but that tracker was limited to a single target.

Bayesian Cramer-Rao bound (BCRB) sets the performance limits on target tracking, providing useful tools for evaluating the effect of system parameters on estimation accuracies. The radar is assumed to be distributed in the sense that targets gains on the paths between transmitters and receivers of the MIMO system are modeled as independent, identically distributed random variables. The results obtained in this chapter assume that realizations of target gains remain fixed throughout the experiment, i.e., a Swerling Type 1 model. Specific contributions are: (1) extension of a MIMO radar indirect tracking scheme originally proposed in [21] for single target to two targets, by incorporating nearest neighbor data association; (2) a new Kalman filter direct tracking scheme for multiple targets, in which tracks are formed and maintained at a fusion center from observations communicated by sensors of a MIMO radar; (3) a new Bayesian Cramer-Rao bound (BCRB) on the performance of the multi-target direct tracking scheme.

The paper is organized as follows: the signal model is formulated in Section II, multiple target tracking algorithms and BCRBs are presented in Section III, numerical examples are presented in Section IV, and concluding remarks are found in Section V. Throughout the paper, matrices are denoted by boldface uppercase letters, and vectors by boldface lowercase letters. The following notations are used: transpose $(\cdot)^T$, complex conjugate transpose $(\cdot)^H$, expectation $E(\cdot)$, absolute value $|\cdot|$, estimated quantities $\widehat{(\cdot)}$, Frobenius norm $\|\cdot\|_F^2$.

2.2 Signal Model

Assume N widely distributed radar receive elements and M widely distributed radar transmit elements that have a common time reference. Each transmitter emits its own waveform with complex envelope $s_m(t), m = 1, ..., M$. The waveforms have unit energy and are orthogonal (for example by being separated in the frequency domain). The power of the transmitted waveforms is normalized such that the aggregate power transmitted by the sensors is constant, irrespective of the number of transmit sensors. Due to the distributed nature of the system, a target's complex gains are assumed multistatic and subsequently modeled as independent random variables. Without loss of generality, assume sensors use pulse Doppler radars in which waveforms of bandwidth B are transmitted at a pulse repetition interval (PRI) T_r. A coherent processing interval (CPI) consists of P pulses, $T_{\text{CPI}} = PT_r$. In a typical implementation, airborne platforms carry single transceivers (i.e., a transmit element and a receive element) forming MN transmit-receive paths. One way to achieve orthogonality of waveforms is to assign sufficiently separated carrier frequencies that may be separated by filtering. Assume there are Q targets, and at the k-th CPI, the q-th target is located at coordinates $\mathbf{p}_k^q = (x_k^q, y_k^q)$ and moves with velocity $\mathbf{v}_k^q = (\dot{x}_k^q, \dot{y}_k^q)$.

The complex envelope of the signal observed at receiver n due to the transmission at transmitter m over time interval $0 \leq t \leq T_{\text{CPI}}$ is given by

$$r_{mn,k}(t) = \frac{1}{\sqrt{M}} \sum_{q=1}^{Q} a_{q,mn} s_m\left(t - \tau_{mn,k}^q\right) e^{j2\pi\mu_{mn,k}^q t} + w_{mn}(t), \tag{2.1}$$

where $a_{q,mn}$ are target complex gains, $\tau_{mn,k}^q$ are time delays, $\mu_{mn,k}^q$ are Doppler shifts, and $w_{mn}(t)$ is circularly symmetric, zero-mean, complex Gaussian with autocorrelation function $\sigma_w^2 \delta(t)$. The normalization by $\sqrt{M}$ ensures that the total transmitted power is independent of the number of emitters. Specifically, $a_{q,mn}$ is the target complex gain associated with the path beginning at the m-th transmit

element, passing through the target q, and ending at the n-th receive element. The propagation time delay associated with state k, transmitter m, receiver n, target q, and location vector $\mathbf{p}_k^q = (x_k^q, y_k^q)$ is given by

$$\tau_{mn,k}^q = \frac{1}{c}\sqrt{(x_{tm} - x_k^q)^2 + (y_{tm} - y_k^q)^2} + \frac{1}{c}\sqrt{(x_{rn} - x_k^q)^2 + (y_{rn} - y_k^q)^2}, \tag{2.2}$$

where (x_{tm}, y_{tm}) denote the coordinates of the m-th transmitting radar and (x_{rn}, y_{rn}) the coordinates of the n-th receiving radar, respectively, and c is the speed of light. The Doppler shift estimate of a signal transmitted on the mn-th path at state k is given by

$$\mu_{mn,k}^q = \frac{f_c}{c}\left[\frac{(x_k^q - x_{tm})\dot{x}_k^q + (y_k^q - y_{tm})\dot{y}_k^q}{\sqrt{(x_{tm} - x_k^q)^2 + (y_{tm} - y_k^q)^2}}\right] + \frac{f_c}{c}\left[\frac{(x_k^q - x_{rn})\dot{x}_k^q + (y_k^q - y_{rn})\dot{y}_k^q}{\sqrt{(x_{rn} - x_k^q)^2 + (y_{rn} - y_k^q)^2}}\right]. \tag{2.3}$$

The term $\dot{x}_k^q$ represents the q-th target velocity along the x-axis and $\dot{y}_k^q$ for the q-th target velocity along the y-axis, at state k.

Let $r_{mn,kp}(t) = r_{mn,k}(t)$, for $(p-1)T_r \leq t \leq pT_r$ and $p = 1, ..., P$. Analysis in the frequency domain is more convenient than in the time domain because in the frequency domain, the time delays appear in the argument of the complex exponential function. To make use of properties of the Fourier transform, we convert the time domain measurements to the frequency domain. The ℓ-th Fourier coefficient of the observed signal at the mn-th path at state k is given by:

$$\widetilde{r}_{mn,k}(\ell, p) = \frac{1}{\sqrt{T_r}}\int_0^{T_r} r_{mn,kp}(t)\, e^{-j2\pi\ell t/T_r} dt. \tag{2.4}$$

Using previously defined quantities, it is not difficult to show that the frequency representation of the received signal is

$$\widetilde{r}_{mn,k}(\ell, p) = \frac{1}{\sqrt{M}}\sum_{q=1}^{Q} a_{q,mn} e^{-j2\pi lp} e^{j2\pi\mu_{mn,k}^q pT_r} \times e^{-j2\pi l\tau_{mn,k}^q/T_r} + \widetilde{w}_{mn}(\ell, p), \tag{2.5}$$

for $\ell = 1, ..., L$ and $p = 1, ..., P$. In (2.5), $\widetilde{w}_{mn}(\ell, p)$ is the Fourier coefficient of $w_{mn}(t)$ in (2.1). Note that $\mathrm{E}\left[|\widetilde{w}_{mn}(\ell, p)|^2\right] = \sigma_w^2$. For later use, define the $MNLP \times 1$ received

vector at state k,

$$\widetilde{\mathbf{r}}_k = \left[\widetilde{\mathbf{r}}_{11,k}^T, ..., \widetilde{\mathbf{r}}_{MN,k}^T\right]^T \tag{2.6}$$

where $\widetilde{\mathbf{r}}_{mn,k} = [\widetilde{r}_{mn,k}(1,1), ..., \widetilde{r}_{mn,k}(L,P)]^T$.

Having formulated the signal model (2.5), we proceed now to define the system state model. To this end, define the 4×1 state vector $\mathbf{x}_k$,

$$\mathbf{x}_k = [x_k, y_k, \dot{x}_k, \dot{y}_k]\,. \tag{2.7}$$

If there are multiple targets, then the dimension of $\mathbf{x}_k$ would be $4Q \times 1$. We continue to write the model for single target. Extension to Q targets is straight forward. The kinematic model is given by

$$\mathbf{x}_{k+1} = \mathbf{F}\mathbf{x}_k + \mathbf{v}_k, \tag{2.8}$$

where $\mathbf{F}$ is the transition matrix

$$\mathbf{F} = \begin{bmatrix} 1 & 0 & PT_r & 0 \\ 0 & 1 & 0 & PT_r \\ 0 & 0 & 1 & 0 \\ 0 & 0 & 0 & 1 \end{bmatrix}, \tag{2.9}$$

and $\mathbf{v}_k$ is modeled as white Gaussian process noise with covariance matrix:

$$\mathbf{Q}_v = \begin{bmatrix} \frac{1}{3}(PT_r)^3 & 0 & \frac{1}{2}(PT_r)^2 & 0 \\ 0 & \frac{1}{3}(PT_r)^3 & 0 & \frac{1}{2}(PT_r)^2 \\ \frac{1}{2}(PT_r)^2 & 0 & PT_r & 0 \\ 0 & \frac{1}{2}(PT_r)^2 & 0 & PT_r \end{bmatrix}. \tag{2.10}$$

The observation model is a non-linear function of the vector of state model:

$$\mathbf{y}_k = \mathbf{H}_k\mathbf{x}_k + \mathbf{w}_k, \tag{2.11}$$

where $\mathbf{H}_k = [\nabla_{\mathbf{x}_k} \mathbf{d}(\mathbf{x}_k)]_{\mathbf{x}_k = \widehat{\mathbf{x}}_k}$ is the linearization matrix that transforms the state vector into the observations vector, $\mathbf{y}_k$ is a suitably defined observations vector, $\mathbf{d}(\cdot)$ captures the non-linear relation between the observations $\mathbf{y}_k$ and the state $\mathbf{x}_k$, and $\mathbf{w}_k$ is complex-valued, additive Gaussian noise process with covariance matrix $\mathbf{R}$.

The extended Kalman filter addresses the problem of estimating state $\mathbf{x}_k$ of a discrete-time controlled process described by the kinematic model (2.8) and observation model (2.11). The following quantities are defined for later use: the filtered estimated state vector $\widehat{\mathbf{x}}_{k|k}$, the predicted state vector $\widehat{\mathbf{x}}_{k|k-1}$, and the associated covariance matrices $\mathbf{P}_{k|k}$ and $\mathbf{P}_{k|k-1}$, respectively. Specific expressions for the computation of these quantities as part of a Kalman filter are given in the next section.

2.3 Multiple Target Tracking

In this section, two tracking algorithms are proposed, both based on the extended Kalman filter.

2.3.1 Indirect Tracking

Indirect techniques require a preliminary stage where TOAs and Doppler frequencies are first estimated at the receiving radars, and then transmitted to the fusion center, where localization is subsequently estimated by multilateration. This estimation approach incorporates at state k an intermediate step of estimating the unknown delay and velocity associated with each path and target. For $m = 1, ..., M$, $n = 1, ..., N$ and $q = 1, ..., Q$, the delay estimates are given by,

$$\widehat{\tau}^q_{mn,k} = \arg\max_{\tau^q_{mn,k}} \left| \sum_{\ell=1}^{L} \sum_{p=1}^{P} \widetilde{r}_{mn,k}(\ell, p) e^{j2\pi l \tau^q_{mn,k}/T_r} \right|. \tag{2.12}$$

Similarly, the Doppler shift estimates for the mn-path of target q at state k is given by:

$$\widehat{\mu}^q_{mn,k} = \arg\max_{\mu^q_{mn,k}} \left| \sum_{\ell=1}^{L} \sum_{p=1}^{P} \widetilde{r}_{mn,k}(\ell, p) e^{-j2\pi\mu^q_{mn,k} p T_r} \right|. \tag{2.13}$$

The 4×1 state vector for target q is $\mathbf{x}^q_k = [x^q_k, y^q_k, \dot{x}^q_k, \dot{y}^q_k]$, and the associated 4×4 covariance matrices are $\mathbf{P}^q_{k|k}$. The transition matrix for each target is $\mathbf{F}$ as given in (2.9). The observation vector for indirect tracking with dimension $2MN \times 1$ is defined as:

$$\mathbf{y}^q_k = \left[\widehat{\tau}^q_{11,k}, \widehat{\mu}^q_{11,k}, ..., \widehat{\tau}^q_{MN,k}, \widehat{\mu}^q_{MN,k}\right]. \tag{2.14}$$

For indirect tracking, the $2MN \times 4$ linearized matrix $\mathbf{H}^q_k$ in the observation model (2.11) is defined as:

$$\mathbf{H}^q_k = \left[\nabla_{\mathbf{x}_k} \mathbf{d}\left(\mathbf{x}_k\right)\right]_{\mathbf{x}_k = \widehat{\mathbf{x}}^q_k}. \tag{2.15}$$

Elements of matrices $\mathbf{H}^q_k$ are found from the derivative of the expressions in equations (2.2) and (2.3) with respect to the state vector in (2.8).

To fully characterize the observation model for the indirect tracker, we need to define the $2MN \times 2MN$ measurement covariance matrix $\mathbf{R}$. For the indirect tracker, for which the observation (3.9) consists of delays and Doppler shift estimates, the measurement covariance matrix $\mathbf{R}$ contains the estimation errors of the delays and Doppler shifts. The matrix $\mathbf{R}$ serves as an input to the tracker, and thus has to be derived extraneous to the tracker. In this work, we populate $\mathbf{R}$ with values of the CRB for delay and Doppler shift estimation. Based on [39], it is not difficult to show that for the signal model (2.6), the $MN \times MN$ Fisher information matrix for delay estimation is given by

$$\mathbf{J}_\tau = \frac{8\pi^2 P^2 B^2}{\sigma^2_w} \text{diag}\left(|a_{q,11}|^2, ..., |a_{q,MN}|^2\right), \tag{2.16}$$

and the $MN \times MN$ Fisher information matrix for Doppler shift estimation is given by

$$\mathbf{J}_{\mu} = \frac{8\pi^2 T_{\text{CPI}}^2}{\sigma_w^2} \text{diag}\left(|a_{q,11}|^2, ..., |a_{q,MN}|^2\right). \tag{2.17}$$

From (2.55) and (2.56), the measurement covariance matrix $\mathbf{R}$ is defined for targets $q = 1, 2$

$$\mathbf{R}^q = \text{diag}(\mathbf{J}_{\tau}, \mathbf{J}_{\mu}). \tag{2.18}$$

For later use in the the tracking algorithm, we define the $2MN \times 2MN$ innovation matrix $\mathbf{K}_k^q$ and the $4 \times 2MN$ Kalman gain matrix $\mathbf{G}_k^q$. Both matrices are used in computations of the filtered estimated state vector $\widehat{\mathbf{x}}_{k|k}$ and the associated covariance matrix $\mathbf{P}_{k|k}$.

Data association techniques utilize a cost function, which is used to base the assignment of observations to tracks. The cost function is the equation which measures how likely new information is to belong to old information. In this work, we apply nearest neighbor assignment. Given the $2MN \times 1$ observation vectors $\mathbf{y}_k^1, \mathbf{y}_k^2$ according to (3.9), the nearest neighbor cost function is $\left[\mathbf{y}_k^u - \mathbf{H}_k^v \widehat{\mathbf{x}}_{k|k-1}^v\right]^H \mathbf{K}_k^v \left[\mathbf{y}_k^u - \mathbf{H}_k^v \widehat{\mathbf{x}}_{k|k-1}^v\right]$ for $u, v = 1, 2$, and where the various quantities (other than the observations) are evaluated as part of the tracking algorithm, as detailed below. The details of the indirect tracking algorithm for a two targets scenario are listed in Table 1 below.

Table 1 Indirect Tracking Algorithm for Two Targets

Input: Measurements $\mathbf{y}_k^1$, $\mathbf{y}_k^2$; $\mathbf{R}^1$, $\mathbf{R}^2$ from (3.10); $\mathbf{P}_{0|0}^1 = \left[\mathbf{H}_0^1(\mathbf{R}^1)^{-1}(\mathbf{H}_0^2)^T\right]^{-1}$, $\mathbf{P}_{0|0}^2 = \left[\mathbf{H}_0^2(\mathbf{R}^2)^{-1}(\mathbf{H}_0^2)^T\right]^{-1}$

1: *Initialization*: Compute by multilateration $\widehat{\mathbf{x}}_{0|0}^1$ based on $\mathbf{y}_0^1$ and $\widehat{\mathbf{x}}_{0|0}^2$ based on $\mathbf{y}_0^2$

2: At time k:

$$\widehat{\mathbf{x}}_{k|k-1}^q = \mathbf{F}\widehat{\mathbf{x}}_{k-1|k-1}^q \tag{2.19}$$

$$\mathbf{P}_{k|k-1}^q = \mathbf{F}\mathbf{P}_{k-1|k-1}^q\mathbf{F}^T + \mathbf{Q}_v \tag{2.20}$$

$$\mathbf{K}_k^q = \mathbf{H}_k^q\mathbf{P}_{k|k-1}^q(\mathbf{H}_k^q)^T + \mathbf{R}^q \tag{2.21}$$

$$\mathbf{G}_k^q = \mathbf{P}_{k|k-1}^q(\mathbf{H}_k^q)^T\left(\mathbf{K}_k^q\right)^{-1} \tag{2.22}$$

Nearest neighbor track association: compute $\left[\mathbf{y}_k^u - \mathbf{H}_k^v\widehat{\mathbf{x}}_{k|k-1}^v\right]^T \mathbf{K}_k^v \left[\mathbf{y}_k^u - \mathbf{H}_k^v\widehat{\mathbf{x}}_{k|k-1}^v\right]$ for $u, v = 1, 2$ and associate measurement to track based on smaller distance

Output:

$$\widehat{\mathbf{x}}_{k|k}^q = \widehat{\mathbf{x}}_{k|k-1}^q + \mathbf{G}_k^q\left(\mathbf{y}_k^q - \mathbf{H}_k^q\widehat{\mathbf{x}}_{k|k-1}^q\right) \tag{2.23}$$

$$\mathbf{P}_{k|k}^q = \mathbf{P}_{k|k-1}^q + \mathbf{G}_k^q\mathbf{K}_k^q(\mathbf{G}_k^q)^T \tag{2.24}$$

2.3.2 Direct Tracking

In the direct tracking approach, observations collected by the sensors are sent to the fusion center, where they are jointly processed to produce localization information and tracks without an intermediate step of estimating the unknown delay and velocity associated with each path and target. In the direct tracking problem, the $4Q \times 1$

compound-target state vector $\mathbf{x}_k$ of Q targets is defined as:

$$\mathbf{x}_k = \left[(\mathbf{x}_k^1)^T, ..., (\mathbf{x}_k^Q)^T \right]^T . \tag{2.25}$$

The transition matrix $\mathbf{F}$ is a $4Q \times 4Q$ block matrix with diagonal blocks given by (2.9), and the $4Q \times 4Q$ process noise covariance matrix $\mathbf{Q}_v$ is a block diagonal matrix with diagonal blocks given by (2.10). The $4Q \times 4Q$ covariance matrix at state k is defined as:

$$\mathbf{P}_{k|k} = E\left[(\mathbf{x}_k - \widehat{\mathbf{x}}_k)(\mathbf{x}_k - \widehat{\mathbf{x}}_k)^T \right]. \tag{2.26}$$

The $MNLP \times 1$ observation vector is defined by,

$$\mathbf{y}_k = \widetilde{\mathbf{r}}_k, \tag{2.27}$$

where $\widetilde{\mathbf{r}}_k$ is given in (2.6). The $MNLP \times 4Q$ measurement matrix $\mathbf{H}_k$ for direct tracking is obtained from the relation

$$\mathbf{H}_k = \left[\nabla_{\mathbf{x}_k} \mathbf{d}\left(\mathbf{x}_k\right) \right]_{\mathbf{x}_k = \widehat{\mathbf{x}}_k} .$$

Elements of matrices $\mathbf{H}_k$ are found from the derivative of the expressions in (2.5) with respect to the compound state vector in (2.50). The estimation error covariance matrix of the noise for direct measurements of received signal with dimension $MNLP \times MNLP$ is $\mathbf{R} = \sigma_w^2 \mathbf{I}_{4Q \times 4Q}$. For later use in the tracking algorithm, we define the $MNLP \times MNLP$ innovation matrix $\mathbf{K}_k$ and the $4Q \times MNLP$ Kalman gain matrix $\mathbf{G}_k$.

The algorithm is initialized with the state estimate of the Q targets. The $4Q \times 1$ state estimate vector $\mathbf{x}_{0|0}$ of Q targets at initialization is given by,

$$\widehat{\mathbf{x}}_{0|0} = \underset{\mathbf{x}_0}{\text{maximize}} \quad \left| \sum_{m=1}^{M} \sum_{n=1}^{N} \sum_{\ell=1}^{L} \sum_{p=1}^{P} \left[\mathbf{y}_k\right]_{m,n,l,p} e^{j2\pi l \tau_{mn,k}^q(\mathbf{x}_0)/T_r} e^{-j2\pi \mu_{mn,k}^q(\mathbf{x}_0) p T_r} \right| \quad , \tag{2.28}$$

where $[\mathbf{y}_k]_{m,n,l,p}$ is the $mnlp$-component of vector $\mathbf{y}_k$.The details of the direct tracking algorithm for a two targets scenario are listed in Table 2 below.

Table 2 Direct Tracking Algorithm for Two Targets

Input: Measurements $\mathbf{y}_k$; $\mathbf{R} = \sigma_w^2 \mathbf{I}_{4Q\times 4Q}$; $\mathbf{P}_{0|0} = \left[\mathbf{H}_0 \mathbf{R}^{-1} (\mathbf{H}_0)^T\right]^{-1}$

1: *Initialization*: Compute $\widehat{\mathbf{x}}_{0|0}$ from (2.28) and (2.50)

2: At time k :

$$\widehat{\mathbf{x}}_{k|k-1} = \mathbf{F}\widehat{\mathbf{x}}_{k-1|k-1} \tag{2.29}$$

$$\mathbf{P}_{k|k-1} = \mathbf{F}\mathbf{P}_{k-1|k-1}\mathbf{F}^T + \mathbf{Q} \tag{2.30}$$

$$\mathbf{K}_k = \mathbf{H}_k \mathbf{P}_{k|k-1}\mathbf{H}_k^T + \mathbf{R}_k \tag{2.31}$$

$$\mathbf{G}_k = \mathbf{P}_{k|k-1}\mathbf{H}_k^T \mathbf{K}_k^{-1} \tag{2.32}$$

$$\widehat{\mathbf{x}}_{k|k} = \widehat{\mathbf{x}}_{k|k-1} + \mathbf{G}_k \left[\mathbf{y}_k - \mathbf{H}_k \widehat{\mathbf{x}}_{k|k-1}\right] \tag{2.33}$$

$$\mathbf{P}_{k|k} = \mathbf{P}_{k|k-1} + \mathbf{G}_k \mathbf{K}_k \mathbf{G}_k^T \tag{2.34}$$

Output: $\widehat{\mathbf{x}}_{k|k}, \mathbf{P}_{k|k}$. There is no data association problem for this tracking algorithm.

2.4 Bayesian Cramer-Rao Bound (BCRB) for Target Tracking

In this section, we derive BCRBs for indirect and direct tracking given the state model formulated in the previous section. The BCRB for an unknown vector parameter $\mathbf{x}$ estimated from an observation vector $\mathbf{y}$ is defined as the inverse of the Bayesian information matrix (BIM) $\mathbf{J}_B^{-1}(\mathbf{x})$ [40], where the BIM is defined

$$\mathbf{J}_B(\mathbf{x}) = E_{\mathbf{y},\mathbf{x}}\left[-\frac{\partial^2}{\partial \mathbf{x} \partial \mathbf{x}^T} \log p_{\mathbf{y},\mathbf{x}}(\mathbf{y},\mathbf{x})\right]. \tag{2.35}$$

The BCRB is a lower bound in the following sense,

$$E_{\mathbf{x},\mathbf{y}}\left([\widehat{\mathbf{x}}(\mathbf{y}) - \mathbf{x}][\widehat{\mathbf{x}}(\mathbf{y}) - \mathbf{x}]^T\right) \geq \mathbf{J}_B^{-1}(\mathbf{x}), \tag{2.36}$$

where the inequality means that the difference between the left- and right-hand sides is a positive semi-definite matrix. We note for later use that the Fisher information matrix is defined

$$\mathbf{J}(\mathbf{x}) = E_{\mathbf{y}|\mathbf{x}}\left[-\frac{\partial^2}{\partial \mathbf{x}\partial \mathbf{x}^T}\log p_{\mathbf{y}|\mathbf{x}}(\mathbf{y}|\mathbf{x})\right]. \tag{2.37}$$

The BCRBs of the individual components of the unknown vector parameter $\mathbf{x} = [x, y, \dot{x}, \dot{y}]$ are obtained from diagonal terms of the inverse BIM $\mathbf{J}_B^{-1}(\mathbf{x})$ denoted as $\left[\mathbf{J}_B^{-1}(\mathbf{x})\right]_{ii}$, $i = 1, ..., 4$.

2.4.1 Direct Tracking for Single Target

In the direct tracking approach, observations collected by the sensors are sent to a fusion center, where they are jointly processed to produce localization information and tracks without the intermediate step of estimating the unknown delay and velocity associated with each path and target. In the direct tracking for single target problem, the 4×1 compound-target state vector $\mathbf{x}_k$ is defined in (2.8). The transition matrix $\mathbf{F}$ is a 4×4 matrix given by (2.9), and the 4×4 process noise covariance matrix $\mathbf{Q}_v$ is given by (2.10). The $MNLP \times 1$ observation vector is given by,

$$\mathbf{y}_k = \widetilde{\mathbf{r}}_k, \tag{2.38}$$

where $\widetilde{\mathbf{r}}_k$ is given in (2.6). The $MNLP \times 4$ measurement matrix $\mathbf{H}_k$ for direct tracking is obtained from the relation

$$\mathbf{H}_k = \left[\nabla_{\mathbf{x}_k}\mathbf{d}\left(\mathbf{x}_k\right)\right]_{\mathbf{x}_k = \widehat{\mathbf{x}}_k}.$$

Elements of matrices $\mathbf{H}_k$ are found from the derivative of the expressions in (2.5) with respect to the state vector in (2.8). It can be shown that:

$$\mathbf{H}_k = \frac{\partial \mathbf{y}_k}{\partial \mathbf{x}_k} = \Big[\begin{array}{cccc} \mathbf{H}_1 & \mathbf{H}_2 & \mathbf{H}_3 & \mathbf{H}_4 \end{array}\Big]_{MNLP \times 4}, \tag{2.39}$$

where

$$[\mathbf{H}_1]_{m,n,l,p} = \left[j2\pi p T_r \frac{f_c}{c} \sin\theta_m - j2\pi f_\ell \frac{1}{c}(\cos\theta_m + \cos\phi_n) \right] \widetilde{r}_{mn,k}(\ell, p), \tag{2.40}$$

$$[\mathbf{H}_2]_{m,n,l,p} = \left[j2\pi p T_r \frac{f_c}{c} \sin\phi_n - j2\pi f_\ell \frac{1}{c}(\sin\theta_m + \sin\phi_n) \right] \widetilde{r}_{mn,k}(\ell, p), \tag{2.41}$$

$$[\mathbf{H}_3]_{m,n,l,p} = j2\pi p T_r \frac{f_c}{c} \left[\frac{\sin^2\theta_m \dot{x}_k - \sin(\theta_m)\cos(\theta_m)\dot{y}_k}{\sqrt{(x_{tm}-x_k)^2+(y_{tm}-y_k)^2}} + \frac{\sin^2\phi_n \dot{x}_k - \sin(\phi_n)\cos(\phi_n)\dot{y}_k}{\sqrt{(x_{rn}-x_k)^2+(y_{rn}-y_k)^2}} \right] \widetilde{r}_{mn,k}(\ell, p), \tag{2.42}$$

$$[\mathbf{H}_4]_{m,n,l,p} = j2\pi p T_r \frac{f_c}{c} \left[\frac{\sin^2\phi_n \dot{x}_k - \sin(\phi_n)\cos(\phi_n)\dot{y}_k}{\sqrt{(x_{tm}-x_k)^2+(y_{tm}-y_k)^2}} + \frac{-\sin(\phi_n)\cos(\phi_n)\dot{x}_k + \cos^2\phi_n \dot{y}_k}{\sqrt{(x_{rn}-x_k)^2+(y_{rn}-y_k)^2}} \right] \widetilde{r}_{mn,k}(\ell, p). \tag{2.43}$$

Here the indexes are $m = 1, ..., M, n = 1, .., N, \ell = 1, ..., L, p = 1, ..., P$. θ_m is the bearing angle of the target at transmitting sensor m and ϕ_n is the bearing angle of the target at receiving radar n measured with respect to the $x-$axis. In mathematical form, $\theta_m = \tan^{-1}\left(\frac{y_k - y_{tm}}{x_k - x_{tm}}\right)$ and $\phi_n = \tan^{-1}\left(\frac{y_k - y_{rn}}{x_k - x_{rn}}\right)$.

The $MNLP \times MNLP$ covariance matrix $\mathbf{R}$ of the noise in the observations model is $\mathbf{R} = \sigma_w^2 \mathbf{I}_4$. The evaluation of BCRB $\mathbf{J}_B(\mathbf{x}_k)$ in (2.35) may be carried out recursively [41],

$$\mathbf{J}_B(\mathbf{x}_k) = \mathbf{D}_k^{22} - \mathbf{D}_k^{21} \left[\mathbf{J}_B(\mathbf{x}_{k-1}) + \mathbf{D}_k^{11} \right]^{-1} \mathbf{D}_k^{12}, \tag{2.44}$$

where

$$\mathbf{D}_k^{11} = \mathbf{F}^T \mathbf{Q}_v^{-1} \mathbf{F}, \tag{2.45}$$

$$\mathbf{D}_k^{12} = -\mathbf{F}^T \mathbf{Q}_v^{-1} = \left[\mathbf{D}_k^{21} \right]^T, \tag{2.46}$$

and

$$\mathbf{D}_k^{22} = \mathbf{Q}_v^{-1} + \mathbf{J}(\mathbf{x}_k). \tag{2.47}$$

In the above equations, $\mathbf{J}(\mathbf{x}_k)$ is the standard Fisher information matrix, which may be expressed as [21],

$$\mathbf{J}(\mathbf{x}_k) = \mathbf{H}_k^T \mathbf{R}^{-1} \mathbf{H}_k. \tag{2.48}$$

Combining (23)-(26) and substituting in (22), the BIM recursion is then given by

$$\mathbf{J}_B(\mathbf{x}_k) = [\mathbf{Q}_v + \mathbf{F}\mathbf{J}_B(\mathbf{x}_{k-1})\mathbf{F}^T]^{-1} + \mathbf{H}_k^T \mathbf{R}^{-1} \mathbf{H}_k. \tag{2.49}$$

The recursion is initialized according to
$\mathbf{J}_B(\mathbf{x}_0) = \mathbf{Q}_v^{-1} + (\mathbf{H}_0)^T(\mathbf{R})^{-1}\mathbf{H}_0$, where $\mathbf{H}_0$ is the linearization matrix (16) taken values at CPI $k = 0$.

2.4.2 Direct Tracking for Multiple Targets

In the direct tracking problem, the $4Q \times 1$ compound-target state vector $\mathbf{x}_k$ of Q targets is defined as:

$$\mathbf{x}_k = \left[(\mathbf{x}_k^1)^T, ..., (\mathbf{x}_k^Q)^T \right]^T. \tag{2.50}$$

The transition matrix $\mathbf{F}$ is a $4Q \times 4Q$ block matrix with diagonal blocks given by (2.9), and the $4Q \times 4Q$ process noise covariance matrix $\mathbf{Q}_v$ is a block diagonal matrix with diagonal blocks given by (2.10). The observation noise covariance matrix for Q targets is given by $\mathbf{R} = \sigma_w^2 \mathbf{I}_{4Q \times 4Q}$. Elements of matrices $\mathbf{H}_k$ are found from the derivative of the expressions in (2.5) with respect to the state vector in (2.50).

The evaluation of BCRB $\mathbf{J}_B(\mathbf{x}_k)$ is carried out recursively using (2.49) with all the parameters for multiple targets are obtained from the same parameters for single target as outlined above.

2.4.3 Indirect Tracking for Single Target

Indirect techniques require a preliminary stage where time of arrivals (TOAs) and Doppler frequencies are first estimated at the receiving radars, and then transmitted

to the fusion center, where localization is subsequently estimated by multi-lateration. This estimation approach incorporates at CPI k an intermediate step of estimating the unknown delay and velocity associated with each path and target. For $m = 1, ..., M$, $n = 1, ..., N$ and $q = 1, ..., Q$, the delay estimates are given by,

$$\widehat{\tau}^q_{mn,k} = \arg\max_{\tau^q_{mn,k}} \left| \sum_{\ell=1}^{L} \sum_{p=1}^{P} \widetilde{r}_{mn,k}(\ell, p) e^{j2\pi l \tau^q_{mn,k}/T_r} \right|. \tag{2.51}$$

Similarly, the Doppler shift estimates for the mn-path of target q at state k are given by:

$$\widehat{\mu}^q_{mn,k} = \arg\max_{\mu^q_{mn,k}} \left| \sum_{\ell=1}^{L} \sum_{p=1}^{P} \widetilde{r}_{mn,k}(\ell, p) e^{-j2\pi \mu^q_{mn,k} p T_r} \right|. \tag{2.52}$$

The 4×1 state vector for target q is $\mathbf{x}^q_k = [x^q_k, y^q_k, \dot{x}^q_k, \dot{y}^q_k]$. The transition matrix for each target is $\mathbf{F}$ as given in (2.9). The observation vector for indirect tracking has dimension $2MN \times 1$ and is defined:

$$\mathbf{y}^q_k = \left[\widehat{\tau}^q_{11,k}, \widehat{\mu}^q_{11,k}, ..., \widehat{\tau}^q_{MN,k}, \widehat{\mu}^q_{MN,k}\right]. \tag{2.53}$$

For indirect tracking, the $2MN \times 4$ linearized matrix $\mathbf{H}^q_k$ in the observation model (2.11) is defined as:

$$\mathbf{H}^q_k = \left[\nabla_{\mathbf{x}_k} \mathbf{d}\left(\mathbf{x}_k\right)\right]_{\mathbf{x}_k = \widehat{\mathbf{x}}^q_k}. \tag{2.54}$$

Elements of matrices $\mathbf{H}^q_k$ are found from the derivative of the expressions in (2.2) and (2.3) with respect to the state vector in (7).

To fully characterize the observation model for the indirect tracker, we need to define the $2MN \times 2MN$ observation covariance matrix $\mathbf{R}$. For the indirect tracker, for which the observation (3.9) consists of delays and Doppler shift estimates, the measurement covariance matrix $\mathbf{R}$ contains the estimation errors of the delays and Doppler shifts. The matrix $\mathbf{R}$ serves as an input to the tracker, and thus has to be derived extraneous to the tracker. In this work, we populate $\mathbf{R}$ with values of the

CRB for delay and Doppler shift estimation. Based on [39], it is not difficult to show that for the signal model (2.5), the $MN \times MN$ Fisher information matrix for delay estimation is given by

$$\mathbf{J}_\tau = \frac{8\pi^2 P^2 B^2}{\sigma_w^2} \text{diag}\left(|a_{q,11}|^2, ..., |a_{q,MN}|^2\right), \tag{2.55}$$

and the $MN \times MN$ Fisher information matrix for Doppler shift estimation is given by

$$\mathbf{J}_\mu = \frac{8\pi^2 T_{\text{CPI}}^2}{\sigma_w^2} \text{diag}\left(|a_{q,11}|^2, ..., |a_{q,MN}|^2\right). \tag{2.56}$$

From (2.55) and (2.56), the measurement covariance matrix $\mathbf{R}$ for targets q is given by

$$\mathbf{R}^q = \text{diag}(\mathbf{J}_\tau, \mathbf{J}_\mu). \tag{2.57}$$

The evaluation of $\mathbf{J}_B(\mathbf{x}_k)$ may be carried out recursively [41], under some conditions met by our model, such as independent process and measurement noise. For the indirect tracker, it is shown in [21] that the recursive BCRB is of the form

$$\mathbf{J}_B(\mathbf{x}_k^q) = \left[\mathbf{Q}_v + \mathbf{F}\mathbf{J}_B(\mathbf{x}_{k-1}^q)\mathbf{F}^T\right]^{-1} + \mathbf{J}(\mathbf{x}_k^q). \tag{2.58}$$

where $\mathbf{J}(\mathbf{x}_k)$ is the standard Fisher information matrix, defined in (2.37). The FIM $\mathbf{J}(\mathbf{x}_k)$ is derived using the chain rule

$$\mathbf{J}(\mathbf{x}_k^q) = (\mathbf{H}_k^q)^T (\mathbf{R}^q)^{-1} \mathbf{H}_k^q. \tag{2.59}$$

Putting it all together, the BIM recursion for the indirect tracker is expressed,

$$\mathbf{J}_B(\mathbf{x}_k^q) = \left[\mathbf{Q}_v + \mathbf{F}\mathbf{J}_B(\mathbf{x}_{k-1}^q)\mathbf{F}^T\right]^{-1} + (\mathbf{H}_k^q)^T (\mathbf{R}^q)^{-1} \mathbf{H}_k^q. \tag{2.60}$$

The recursion is initialized as $\mathbf{J}_B(\mathbf{x}_0^q) = \mathbf{Q}_v^{-1} + (\mathbf{H}_0^q)^T (\mathbf{R}^q)^{-1} \mathbf{H}_0^q$, where $\mathbf{H}_0^q$ is the linearization matrix (2.54) taken values at CPI $k = 0$. Next, a numerical analysis of

the BCRBs is provided, leading to a better understanding of the tracking performance in MIMO radar systems.

2.5 Numerical Examples

In this section, numerical examples are presented to illustrate the performance of the proposed trackers. We assess the performance of the indirect and direct trackers by means of a normalized localization error. Defining the range resolution in terms of the speed of light c and bandwidth B, $r = c/2B$, and using it as a normalization factor, we define the normalized root-mean-square error for target q at state k as:

$$\text{rMSE}_k^q = \frac{1}{rZ} \sum_{z=1}^{Z} \sqrt{[(\widehat{x}_{k,z}^q - x_{k,z}^q)^2 + (\widehat{y}_{k,z}^q - y_{k,z}^q)^2]}, \tag{2.61}$$

where Z is the the number of Monte Carlo experiments, $(\widehat{x}_{k,z}^q, \widehat{y}_{k,z}^q)$ is the q-target's location estimate of the state model $(x_{k,z}^q, y_{k,z}^q)$ for the z-th repetition.

The BCRBs in this case are the lower bounds on the normalized localization error and can be defined as:

$$\text{BCRB}_k^q = \frac{1}{rZ} \sum_{z=1}^{Z} \sqrt{\left[\mathbf{J}_B^{-1}(\mathbf{x}_k^q)\right]_{11} + \left[\mathbf{J}_B^{-1}(\mathbf{x}_k^q)\right]_{22}}, \tag{2.62}$$

where $\mathbf{J}_B(\mathbf{x}_k^q)$ for indirect tracking is given in (2.60). For direct tracking the BCRB for target q at state k, $\mathbf{J}_B(\mathbf{x}_k^q)$, is the q-th diagonal block, for $q = 1, 2, .., Q$, of the expression $\mathbf{J}_B(\mathbf{x}_k)$ as given in (2.49).

Assume the transmitted pulse is a rectangular pulse of duration $T_p = 100$ ns, pulse repetition interval $T_r = 100T_p$, $P = 10$, and $L = 100$. The target gains $a_{q,mn}$, for $q = 1, 2, .., Q$, $m = 1, 2, .., M$, $n = 1, 2, .., N$, were modelled as independent, complex Gaussian random variables with $E[|a_{q,mn}|^2] = 1$. Monte Carlo simulations were run over different instantiations of targets gains and noise. The average SNR was assumed $\text{SNR} = 1/\sigma_w^2 = 10$ dB. For the numerical results presented below, the setup consisted of a 2×3 MIMO radar system and two targets as illustrated in Figure 2.1.

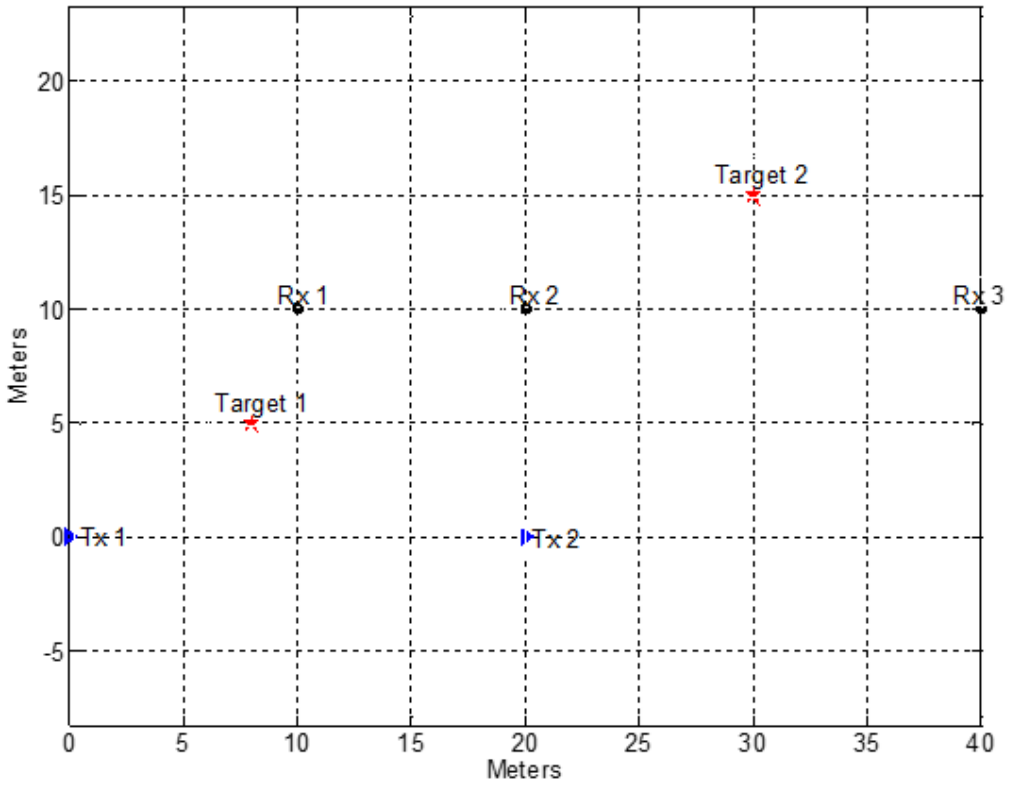

Figure 2.1 Setup used for the simulations: a 2×3 MIMO radar system and two targets.

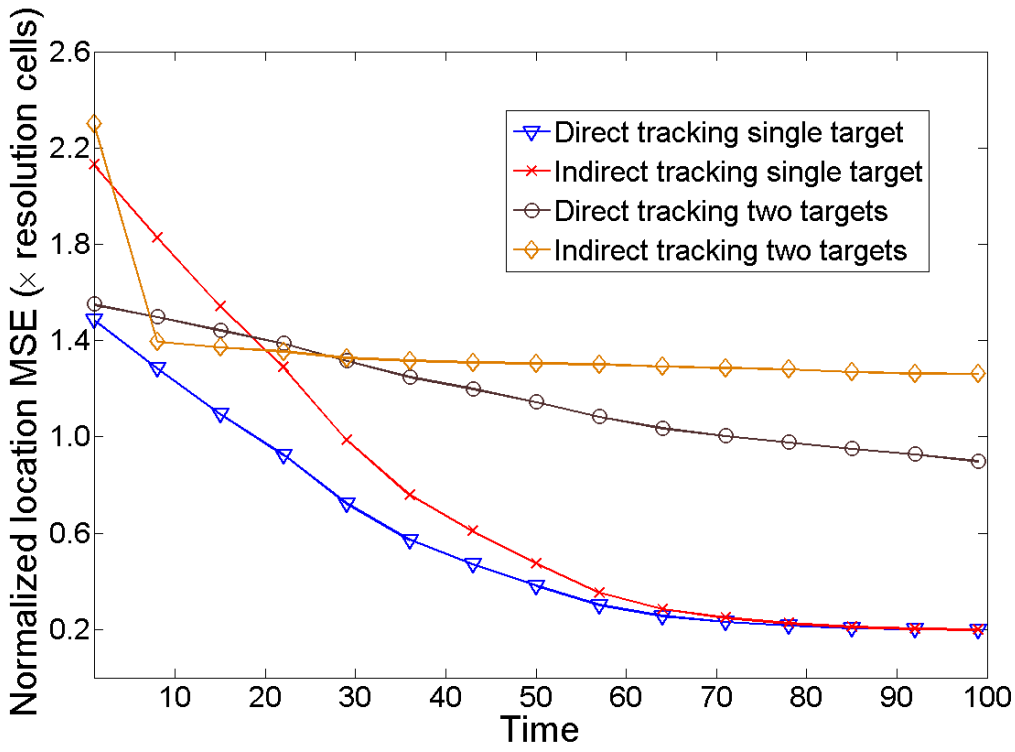

Figure 2.2 Normalized localization error as function of time for tracking one and two targets with indirect and direct tracking.

Figure 2.2 shows the normalized location root-mean-square-error as defined in (2.61) as a function of time, for indirect and direct tracking of single and two targets. It is observed that direct tracking provides better performance at low SNRs for a single target and at all SNRs for multiple targets.

Figure 2.3 shows the performance of the trackers for single and two targets as obtained from simulations and BCRBs. The BCRB for indirect tracking is given in (2.60) and the BCRB for direct tracking is given in (2.49). BCRBs are averaged over the target gains and are plotted as a function of time using (2.62), for indirect and direct tracking of single and two targets. It is shown in Figure 2.2 that, the extended Kalman filter achieves the BCRB asymptotically, hence the trackers for both direct and indirect cases perform efficiently [39].

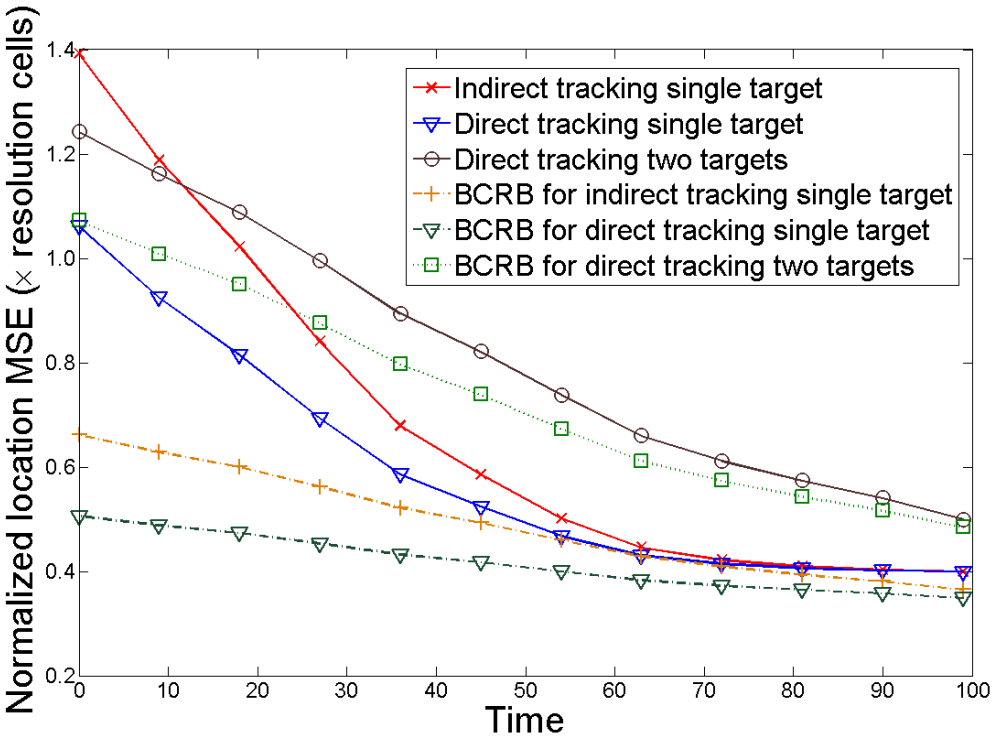

Figure 2.3 Normalized localization error BCRBs as function of time for tracking target(s) with indirect and direct tracking.

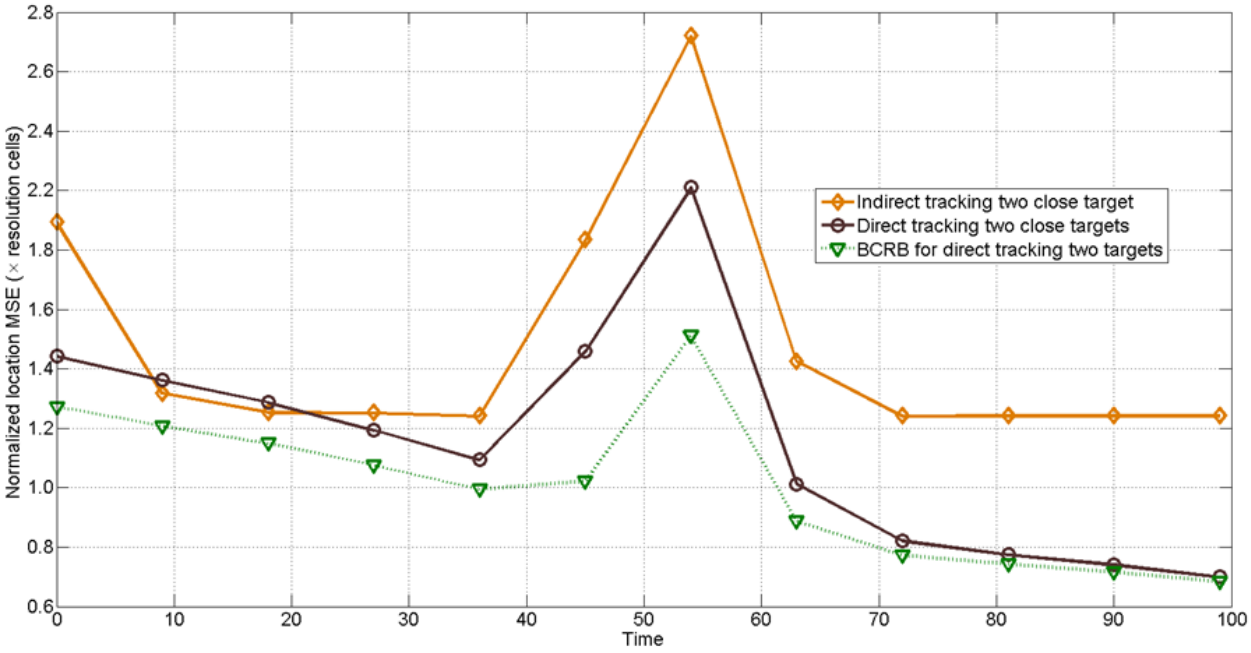

Figure 2.4 Normalized localization error as a function of time for tracking two crossing targets.

Figure 2.4 shows the normalized location root-mean-square-error as defined in (2.61) as a function of time when the two targets are crossing. The BCRB for direct tracking is given in (2.49). It is observed that as the distance between the two targets is becoming smaller, there is an increase in the mean square error. The normalized MSE is reduced when the targets are further separated.

Kalman filter provides the best minimum MSE linear estimator and the extended Kalman filter provides an estimate that is a solution to the unconstrained l_2 minimization problem. In principle, a sparse vector can be recovered from the least number of elements by solving the non-convex combinatorial l_0-norm problem. This constrained optimization problem can be solved in the framework of extended Kalman filtering with additional step using Orthogonal Matching Pursuit (OMP). OMP algorithm try to find the Q non-zero values one at a time and repeats until all Q elements are chosen. Figure 2.5 shows the normalized location root-mean-square-error as defined in (2.61) as a function of time with sparse framework. The BCRB for

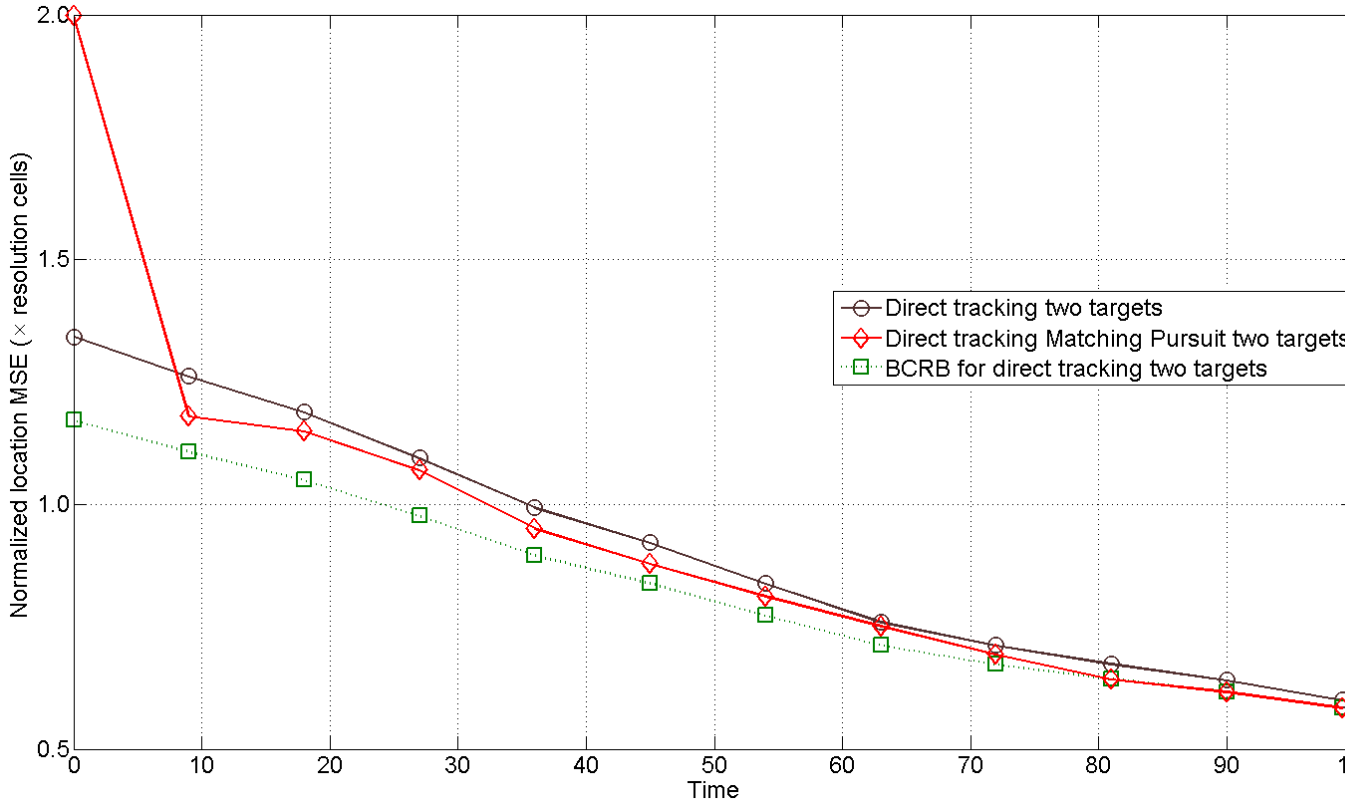

Figure 2.5 Normalized localization error as a function of time for tracking two targets with sparse framework .

direct tracking is given in (2.49). It is observed direct tracking with OMP algorithm improves the performance over regular direct tracking.

2.6 Concluding Remarks

In this chapter we proposed a new approach to solve the multiple moving target tracking problem in MIMO radar systems. Based on this study, two tracking schemes are proposed. The first is an indirect tracking approach, based on time delay and velocity estimates and implicit nearest-neighbor data association at the fusion center. The second is a direct scheme, based on radar observations tracking and the data association of multiple targets is implicit. The later eliminates intermediate estimated parameters and tracks the moving targets with higher accuracy. Numerical results

show that for multiple targets, direct tracking algorithm outperforms indirect tracking at all SNR values.

CHAPTER 3

EFFECT OF PHASE NOISE ON STAP BY SENSORS WITH INDEPENDENT OSCILLATORS

3.1 Introduction

Radars on multiple distributed airborne or ground based moving platforms are of increasing interest, since they can be deployed in close proximity to the event under investigation and thus offer remarkable sensing opportunities [1]. For example, unmanned aerial vehicles (UAVs) based radars play a significant role in disaster relief efforts by quickly flying to the impacted area and providing the most accurate and updated information [2]. In urban sensing environments, potential targets may be obscured by buildings and other man-made structures; with sensors on moving platforms, the subject area can be probed from more favorable positions to yield enhanced detectability [3]. Other applications of radar on moving platforms for military and civilian sensing operations can be found in, e.g., [4], [5], [6].

In ground moving target indicator (GMTI), of interest is to determine the presence of targets and their ranges, azimuth angles, and Doppler shifts. Space-time adaptive processing (STAP) enables GMTI radars to perform moving target detection in the presence of ground clutter. STAP implemented with antenna arrays has been a classical approach to clutter cancellation in airborne radar [22, 23]. The proliferation of airborne, inexpensive radio frequency sensors raises interest in distributed implementation of radar systems. In this work, we consider certain aspects of a distributed implementation of STAP.

The power spectral density (PSD) of an ideal sinusoidal carrier observed over $t \to \infty$ is an impulse at f_0. However, practical oscillators have amplitude and phase deviations from the ideal oscillator that cause spreading of the spectrum. The phase

deviation of a practical oscillator from the nominal phase $2\pi f_0 t$, where f_0 is the carrier frequency is known as phase noise. The study of phase noise has started more than 50 years ago, as reviewed in a recent retrospective [24]. As explained in [24], diverse applications of oscillators led to a variety of analysis approaches. The lack of a unified approach and the difficulty of the topic resulted in a large number of publications, including in the IEEE Proceedings (for example [25, 26, 27, 28], to name a few). Efforts to consolidate and standardize terms yielded an IEEE standard [29] and a National Institute of Standards publication [30].

The characterization and the effects of phase noise on performance have been topics of interest also to the radar community. Phase deviations accumulate over time, hence the effect of phase noise becomes more pronounced over longer observation times. It is not surprising then that a significant body of literature addresses the effect of phase noise on synthetic aperture radar (SAR) [31]-[32]. SAR integration times are long and phase noise may have great effect on performance. Although the observation time is not quite as long as in SAR, Doppler processing may also be affected by phase noise, with publications spanning many years from [33] to [34]. In contrast, literature on the effect of phase noise on antenna arrays is difficult to come by for the simple reason that spatial processing relies on differential phase measurements between array elements. When the same oscillator drives all elements, phase noise effects are canceled. However, in a distributed application, different sensors are driven by different oscillators. Different oscillators develop different phase noise characteristics as a function of time, making the array subject to the effect of phase noise errors. Thus, at a given sensor, the phase noise associated with the sensor's oscillator affects Doppler processing, whereas the phase noise between oscillators at different sensors affects spatial processing.

Besides phase noise, a distributed STAP system it is also subject to other impairments such as frequency offset, non-uniform motion characteristics of individual

sensors, non-uniform and potentially large spacing between array elements, and sensors locations uncertainties, to name a few. Frequency offsets inevitably arise even when all sensors are instructed to tune to the same frequency. Whereas a Doppler shift is caused by relative motion, a carrier frequency offset is caused by the carrier frequency mismatch between transmitter and receiver. A distributed STAP system with is subject to errors from carrier frequency offsets (CFO). In [35], the authors investigate the effect of CFO on Doppler centroid estimation in Synthetic Aperture Radar (SAR) and on Direction-Of-Arrival (DOA) estimation in array processing. To the best of our knowledge, there is no past work done on effect of frequency offset for distributed STAP system.

In addition to frequency offset due to different transmitters and receivers, in a distributed system, different sensors move autonomously, and thus, may have different velocities and direction of motion. This, in turn, leads to Doppler characteristics that vary among sensors. As a result, space-time steering vectors may not be expressed simply by a Kronecker product, as in traditional STAP. In this work, we analyze the generalized motion of target and sensors in a multistatic setup and highlight the effects of platform motion on the clutter problem. Further, classical STAP is typically implemented with uniform linear arrays (ULA), half-wavelength spacing. A distributed implementation leads to non-uniform and potentially much larger spacings between the array elements. Finally, a rigid implementation on a single platform enables to accurately measure the locations of the array's elements. In a distributed implementation, sensors relative locations vary over time, and any sensor localization method (e.g., GPS) is subject to errors. Relevant to analysis of the effect of element errors in a distributed array, is the analysis of the effect of element errors in arrays with colocated elements [36]). In [37], Flanagan achieved array self-calibration with large sensor position errors. Other papers, for example [38], derived the Cramer-Rao lower bounds of the DOA estimation and array calibration precisions in the

case of determined and unknown signals based on the assumptions of small array perturbations.

In this chapter, we study the effect of phase noise and other impairments on STAP with distributed antenna arrays. We envision a STAP application, in which spatial and Doppler processing are performed over a coherent processing interval. Specific contributions are: (1) demonstrate that a power law phase noise PSD model is suitable for analyzing the distributed radar system, (2) propose a simplified time-domain model for the phase noise, (3) develop analytical expressions that quantify the effect of phase noise on the array beampattern as a function of time, (4) propose a generalized motion model for distributed STAP system, (5) demonstrate the effect of phase noise and other impairments on target detection by numerical examples of receiver operating characteristics (ROC). The chapter is organized as follows: the signal model is formulated in Section II, phase noise modelling is presented in Section III, effect of phase noise on STAP is analyzed in Section IV, and performance of distributed STAP is presented in Section V.

3.2 Signal Model

Consider a distributed radar system in which relatively simple sensors on multiple platforms send observations to a fusion center, where most of the baseband processing is performed. The platforms are assumed to move independently with different velocities and directions, but for simplicity of presentation it is assumed that the observation time of interest, the sensors form a linear array. The spacing between the elements of the array may be non-uniform and arbitrary. The distributed sensors are further assumed to be time-synchronized (e.g., with the help of GPS), but not phase synchronized. Let the number of distributed sensors that form the array be N_s. The envisioned application is a STAP system, in which the N_s sensors collect echoes resulting from the transmission of a finite train of N_p coherent pulses. The pulses are

emitted by a single transmitter and feature a T_r pulse repetition interval (PRI). The coherent processing interval (CPI) is then $T_{\text{CPI}} = N_p T_r$. The radar operating carrier wavelength is λ, and the wave number is defined $k_0 = 2\pi/\lambda$. The sensor positions are assumed to be given by the sequence $(z_1, z_2, ..., z_{N_s})$ expressed in units of wavelength. The length of the array aperture is $Z = |z_n - z_1|$.

Let $u = \sin\theta$ denote the spatial frequency associated with the azimuth angle θ measured with respect to the normal to the array. The $N_s \times 1$ spatial steering vector $\mathbf{b}(u)$ represents the noise-free signal received at the array elements from a unit amplitude target at spatial frequency u, and is given by

$$\mathbf{b}(u) = \frac{1}{\sqrt{N_s}}[e^{jk_0 z_1 u}\ e^{jk_0 z_2 u}\ \ldots\ e^{jk_0 z_{N_s} u}]^T. \tag{3.1}$$

Applying the vector $\mathbf{b}^*(u)$ steers the array to spatial frequency u, hence $\mathbf{b}(u)$ is known as a *steering vector*. The spatial array factor is defined

$$\begin{aligned} b_0(u) &= \mathbf{b}^H(u' - u)\mathbf{b}(u') \\ &= \frac{1}{N_s}\sum_{n=1}^{N_s} e^{jk_0 z_n u}. \end{aligned} \tag{3.2}$$

The beampattern is defined as the magnitude of the array factor. The main lobe of the beampattern is the region $|u| \leq 1/Z$, while the sidelobe region is $|u| > 1/Z$.

Since sensors move independently, the Doppler shift due to the sensor-target motion is sensor-dependent. Figure 3.1 shows the parameters associated with the motion of the target and one of the sensors. Since the Doppler shift depends only on the sensor's velocity and direction, and not on its location, the shows the axes origin arbitrarily located at the sensor. The horizontal axis is colinear with the array. Let v_S and γ_S be the sensor's velocity and direction of motion, and v_T and γ_T be the target's likewise parameters. Let $\mathbf{v}_S$ and $\mathbf{v}_T$ be the respective velocity vectors. The target motion relative to the sensor is then $\mathbf{v}_{ST} = \mathbf{v}_S - \mathbf{v}_T$. The magnitude of $\mathbf{v}_{ST}$,

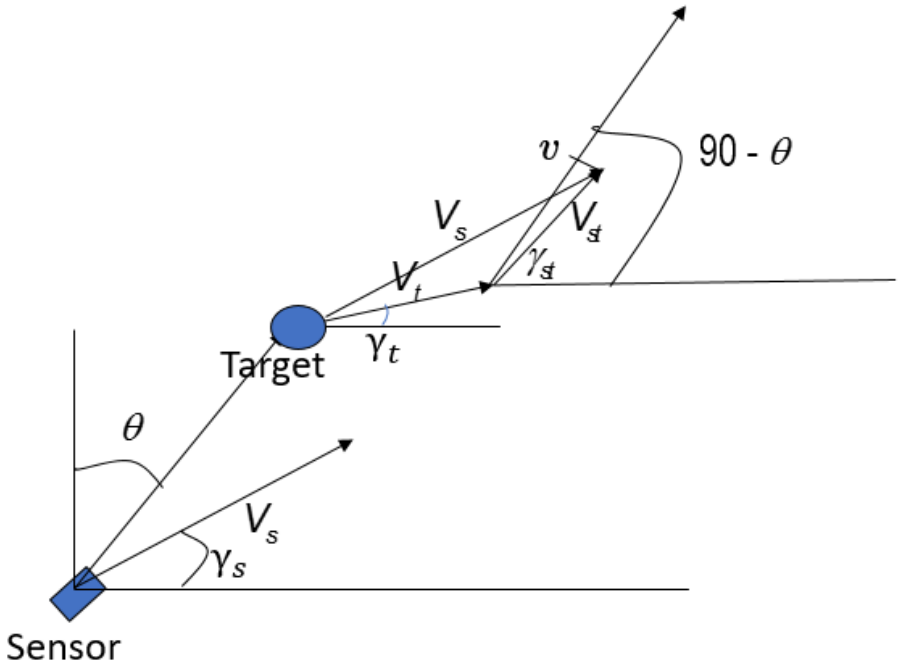

Figure 3.1 Generalized motion for distributed STAP architecture.

v_{ST} is given by the law of cosines

$$v_{ST} = \sqrt{v_S^2 + v_T^2 - 2v_S v_T \cos(\gamma_S - \gamma_T)}. \tag{3.3}$$

and angle of $\mathbf{v}_{ST}$, γ_{ST} is given by the law of sines

$$\gamma_{ST} = 180^o + \gamma_T - \arcsin\left(\frac{v_S}{v_T}\sin\left(\gamma_S - \gamma_T\right)\right). \tag{3.4}$$

It is not difficult to show that the radial velocity between the target and the sensor is given by

$$v = v_{ST}\sin\left(\gamma_{ST} + \theta\right) \tag{3.5}$$

Given a radial velocity v, and letting $f = v/\lambda$ be the normalized frequency, the steering vector formed by time samples has elements with phase function of frequency:

$$\mathbf{d}(f) = \left[1, e^{j2\pi f T_r}, ..., e^{j2\pi(N_p-1)fT_r}\right]^T \tag{3.6}$$

Applying the vector $\mathbf{d}^*(f)$ steers the time samples to frequency f. The Doppler array factor is defined

$$\begin{aligned} d(f) &= \mathbf{d}^H(f' - f)\mathbf{d}(f') \\ &= \frac{1}{N_p}\sum_{m=1}^{N_p} e^{j2\pi(m-1)fT_r}. \end{aligned} \tag{3.7}$$

When elements of the array move independently, the temporal steering vector depends on the motion of the sensor, hence the sensor index n, $1 \leq n \leq N_s$ is added to the notation in (3.7). Let $N = N_s N_p$, then the $N \times 1$ space-time steering vector with spatial frequency u and frequency parameters $f_1 = v_1/\lambda, ..., f_{N_s} = v_{N_s}/\lambda$ is given by

$$\mathbf{a}(u, \mathbf{f}) = \frac{1}{\sqrt{N}}\left[\mathbf{d}^T(f_1)e^{jk_0 z_1 u}, ..., \mathbf{d}^T(f_{N_s})e^{jk_0 z_{N_s} u}\right]^T \tag{3.8}$$

where the argument $\mathbf{f}$ denotes the frequencies $f_1, ..., f_{N_s}$ and the normalization ensures that $\mathbf{a}^H(u, \mathbf{f})\mathbf{a}(u, \mathbf{f}) = 1$. This model of steering vectors implies that while the array is distributed and sensor move independently, targets provide a coherent response across the array from which angle of arrival information may be developed.

After match filtering and sampling, the $N \times 1$ complex vector received at the array from a target at spatial frequency u, Doppler f and complex gain x, and in the presence of clutter $\mathbf{e}_c$ and thermal noise $\mathbf{e}_w$, is expressed

$$\mathbf{y} = x\mathbf{a}(u, \mathbf{f}) + \mathbf{e}_c + \mathbf{e}_w. \tag{3.9}$$

Both $\mathbf{e}_c$ and $\mathbf{e}_w$ are assumed zero mean and Gaussian vectors. It is common to treat the ground clutter and thermal noise as uncorrelated. The $N \times N$ interference covariance matrix $\mathbf{R}$ is then given by

$$\mathbf{R} = \mathbf{E}\left[(\mathbf{e}_c + \mathbf{e}_w)(\mathbf{e}_c + \mathbf{e}_w)^H\right] = \mathbf{R}_c + \mathbf{R}_w. \tag{3.10}$$

Here $\mathbf{R}_w$ is the covariance matrix of the thermal noise given by $\mathbf{R}_w = \sigma^2\mathbf{I}$ where σ^2 is the power of thermal noise. A typical model for the clutter covariance matrix $\mathbf{R}_c$ [2] is

$$\mathbf{R}_c = \int_{-1}^{1} s(u)\mathbf{a}\left(u, \beta u\right)\mathbf{a}^H\left(u, \beta u\right) du \tag{3.11}$$

where s is the power of the clutter scatterer at spatial frequency u with the normalized Doppler frequency $fT_r = \beta u$, $\beta = 4v_S T_r/\lambda$. For high pulse repetition radar for which there is no Doppler aliasing, $\beta = 1$ [22].

The operation of the array is subject to phase errors stemming from sensors driven by independent oscillators. Even assuming perfect calibration at some time instant, phase errors between the sensors develop over time due to the different phase noise contributed by each oscillator. Phase noise is the phase deviation $\phi\left(t\right)$ of a practical oscillator from the nominal phase $2\pi f_0 t$, where f_0 is the carrier frequency. The cumulative effect of the phase noise increases as a function time. In the envisioned STAP setting, the time interval of interest is the CPI time, T_{CPI} defined previously. To incorporate phase noise in our model (3.9), let the diagonal matrix of phase noise processes

$$\mathbf{D} = \text{diag}[e^{j\phi_1(t)}, \ldots, e^{j\phi_{N_s}(t)}], \tag{3.12}$$

where $\phi_n\left(t\right)$ is the phase noise process at the n-th sensor. With phase noise, the signal model becomes

$$\mathbf{y} = x\mathbf{D}\mathbf{a}(u, \mathbf{v}) + \mathbf{e}. \tag{3.13}$$

In the STAP system, the time instants of interest are the sampling times for Doppler processing (slow time) associated with a specific range.

In the next section, we will discuss phase noise model and present some examples of typical oscillators.

3.3 Phase Noise Model

Phase noise of oscillators is modeled as a stochastic process that may be characterized in the time or frequency domains. Time-domain models are suitable for analysis of timing jitter [42, 43, 29], whereas frequency domain models are often used for analysis of short term stability [44, 28, 29]. Next, we review frequency domain characterization of phase noise, present two specific example oscillators, and develop a simple time-domain model suitable for the two oscillators over an observation time of interest.

3.3.1 Frequency-Domain Characterization of Phase Noise

The output of a practical oscillator may be expressed

$$V(t) = V_0 e^{j(2\pi f_0 t + \phi(t))}, \tag{3.14}$$

where f_0 is the carrier frequency and $\phi(t)$ is phase noise. The power spectral density (PSD) of an ideal sinusoidal carrier observed over a time interval $t \to \infty$ is an impulse at f_0. The PSD of $V(t)$ differs from an impulse function, and thus contains information on the effect of phase noise. For the application of interest in this paper, it is reasonable to assume (as illustrated by example later on) that the phase noise meets a small angle approximation, meaning that over the time observation of interest, $|\phi(t)| << 1$, from which it follows that $e^{j\phi(t)} \approx 1 + j\phi(t)$.

It is common for oscillators to be characterized in terms of the PSD of $\phi(t)$ rather than the PSD of $e^{j\phi(t)}$; hence it is important to elucidate the relation between the two PSDs. Accounting for the small angle approximation, the time autocorrelation of the oscillator output is

$$R_V(\tau) = E[V(t)V^*(t-\tau)] = V_0^2 E[(1 + j\phi(t))(1 - j\phi(t-\tau))]. \tag{3.15}$$

If the phase noise process is zero-mean,

$$R_V(\tau) = V_0^2(1 + R_\phi(\tau)), \tag{3.16}$$

where $R_\phi(\tau) = E[\phi(t)\phi(t-\tau)]$. Assuming wide sense stationarity (WSS), the Fourier transform may be applied to obtain,

$$S_V(f_0 + f) = V_0^2 \left(\delta\left(f - f_0\right) + S_\phi(f)\right) \tag{3.17}$$

where $S_V(f_0 + f)$ is the PSD of the oscillator output and $S_\phi(f)$ is the PSD of the phase noise. The relation in (3.17), may be also written

$$S_\phi(f) = \frac{S_V(f_0 + f)}{V_0^2}, \quad f \neq f_0 \tag{3.18}$$

In (3.18), the phase noise PSD is measured in units of dBc/Hz. From this relation, we conclude that the noise PSD $S_\phi(f)$ informs on the effect of phase noise on the oscillator output PSD $S_V(f_0 + f)$.This expression justifies the characterization of oscillators via the PSD of the phase noise rather than the oscillator output, at least in so far as WSS holds. However, as discussed below, in general, phase noise is not WSS. In [45], a relation similar to (3.18) is developed from a direct expansion of $V\left(t\right)$ into its components at various frequencies, without assuming WSS.

Often, an oscillator product sheet provides information on the phase noise power spectral at one frequency f_a, but the PSD is of interest at another frequency f_b. In this case, the power spectral densities are related according to [46]

$$S_\phi(f_b) = S_\phi(f_a) + 20\log\left(\frac{f_b}{f_a}\right) \tag{3.19}$$

One of the best known models for the PSD of phase noise is the Leeson model [27]. This model is a power law model f^ν with three regions $\nu = -3$, $\nu = -2$ and $\nu = 0$. Other models have more terms $\nu \in \{-4, -3, -2, -1, 0, \}$ [47, 48]. Here, we assume that the phase noise PSD follows the model

$$S_\phi(f) = af^{-4} + bf^{-3} + cf^{-2} + df^{-1} + e. \tag{3.20}$$

According to this model, the phase noise process is constituted from multiple independent noise processes. Each process is dominant in a frequency range. The parameters a, b, c, d, e, are related to five different types of noise components.

Random processes whose spectral densities consist of power laws f^ν for $\nu < -1$, are non-integrable as $f \to 0$. It follows that these processes are also not stationary. Such power law processes belong to the class of random processes with stationary n-th increments [49]. For processes with power law PSD, stationarity is met only for a white noise process $\nu = 0$. For white FM noise ($\nu = -2$), the infinite power at low frequency has been resolved by assuming a Lorentzian PSD. Lorentzian is the shape of the power spectrum of stationary white noise passing through a one-pole lowpass filter. Thus, Lorentzian phase noise is stationary and lends itself to analytical expressions. Lorentzian PSD is often assumed in the literature addressing the effect of phase noise on communication systems [50, 51, 52, 53]. However, the Lorentzian model is not necessarily suitable for the longer observation times typical to radar measurements. For example, the effect of phase noise on SAR it typically based on a full power law model, such as (3.20). For further insight on the effect of phase noise on STAP, the analysis and numerical examples in this paper are based on two specific oscillators: an ultra stable oscillator (USO) used in SAR systems as specified in [32], and a lower cost voltage controlled oscillator (VCO), specifically a Wenzel crystal oscillator [54]. The characterization of phase noise for each of the oscillators is discussed below in further detail.

3.3.2 Ultra Stable Oscillator (USO)

USO have a variety of applications in radar. For example, they are used in SAR systems where longer term stability is important [31, 55, 56, 57, 32]. It is of interest to estimate from the spec PSD figure the values of the parameters a through e in the model (3.20). In [58], the authors provided a parametric estimation method to match

the spectrum to the model (3.20). The USO analyzed in this work has the following specification at 10 MHz [32]: $a = -95$ dB, $b = -90$ dB, $c = -200$ dB, $d = -130$ dB, and $e = -155$ dB. Assuming a radar operating at $f_0 = 5$ GHz, and applying (3.19), the following parameters are obtained for the oscillator: $a = -68$ dB, $b = -63$ dB, $c = -173$ dB, $d = -103$ dB, and $e = -128$ dB. Figure 2 shows the composite phase noise PSD characteristic as well each of the components of the power law model of the USO. From the figure it is observed that each component dominates a frequency range in the spectrum. For example, from 1 Hz to 100 Hz, bf^{-3} term is dominant. From 100 Hz to 1000 Hz, the PSD is dominated by the df^{-1}. At higher frequencies, the e term is the strongest.

In the envisioned STAP application, we assume a PRI of the order of milliseconds and a CPI of the order of over 100 milliseconds. This implies that the frequencies of interest are between 1 Hz and 1000 Hz. It is observed from Figure 3.2 that the parameters $\nu = 0$, -1 and -3 are best suited to model the phase noise of the USO in the frequency range $1 \leq f \leq 1000$ Hz. We conclude from that model (3.20) is better suited for this oscillator than the simpler Lorentzian model.

3.3.3 Voltage Controlled Oscillators (VCO)

The VCO was modeled according to the product sheet [54] of a commercial off-the-shelf crystal oscillator. In addition to the phase noise spectrum. The VCO analyzed in this work has the following specification at 10 MHz : $a = -60$ dB, $b = -60$ dB, $c = -90$ dB, $d = -140$ dB, $e = -155$ dB. Converting the power law parameters to 5 GHz, the following coefficients are obtained for power terms in (3.20): $a = -33$ dB, $b = -33$ dB, $c = -63$ dB, $d = -113$ dB, $e = -138$ dB. Figure 4 shows the individual power law components of the phase noise. It is observed from the figure that from 1 Hz to 100 Hz, the af^{-4}, bf^{-3} terms are dominant terms. From 100 Hz to 1 kHz, the bf^{-3}, cf^{-2}, df^{-1} terms dominate. Thus, the VCO requires four power

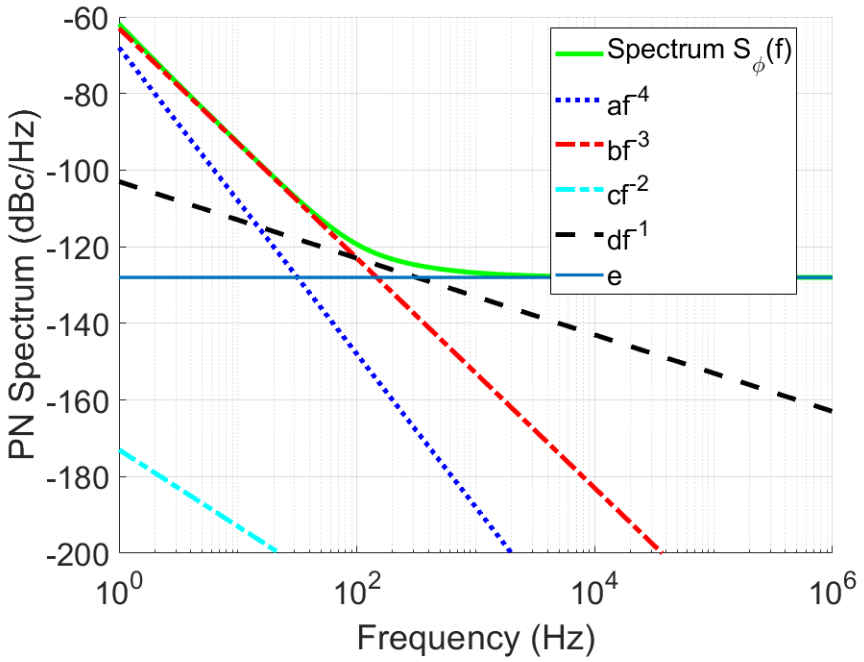

Figure 3.2 Phase noise power spectral density and constituent terms of an USO.

law components to model the phase noise PSD in the frequency range $1 \leq f \leq 1000$ Hz. Again, the simpler Lorentzian model is not suitable.

In conclusion, for both oscillators, it is important to use the full model provided by (3.20), rather than simpler, approximate models used in other applications. However, the PSD (3.20) is not a rational function, and the phase noise process is non-stationary, making difficult to obtain analytical results. Next, we propose a simple time-domain model that holds within the time and frequency parameters relevant to the envisioned STAP application.

3.3.4 Time-Domain Model

To develop the time-domain model, we are interested to generate by simulation time series that exhibit the power law spectrum (3.20). Such a method has been proposed in [59], and recently applied to the simulation of phase noise [60]. Given the PRI T_r, and the CPI $T_{\text{CPI}} = N_p T_r$, M Fourier frequencies are selected such that highest

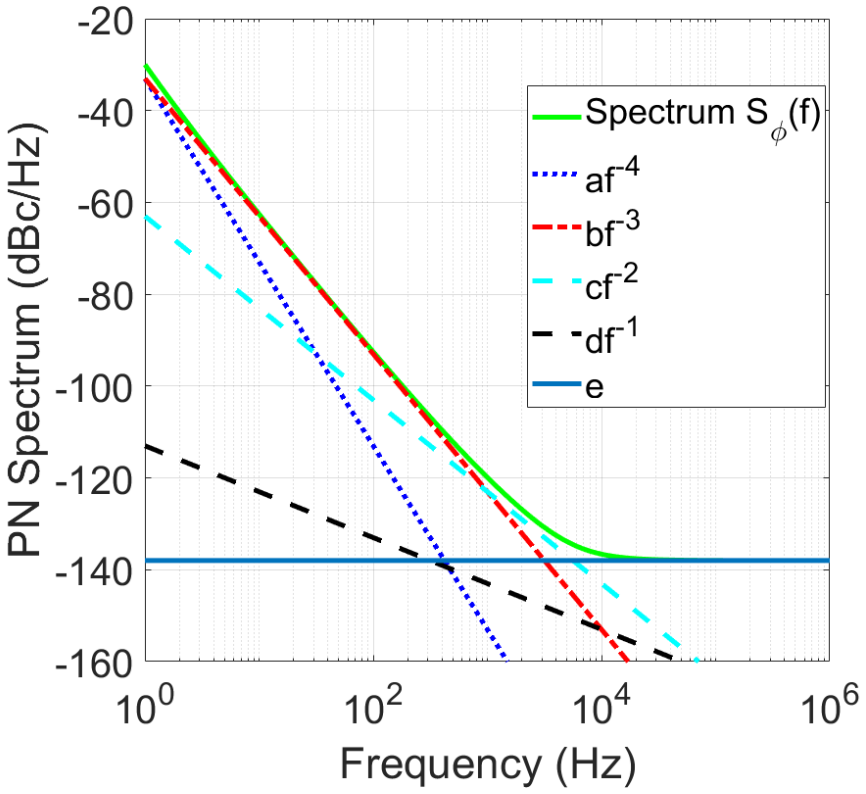

Figure 3.3 Phase noise power spectral density and constituent terms of an VCO.

frequency is $f_{\max} = 1/(2T_r)$, $f_m = (m/M) f_{\max}$, $m = 1, ..., M$ and $M \geq N_p$. For each m, a complex number w_m is drawn from a zero-mean unity variance complex Gaussian distribution. Since the time series representing phase values is real, the complex numbers for the negative frequencies are chosen $w_{-m} = w_m^*$. A frequency domain series of length $2M$ is obtained multiplying w_m by $\sqrt{S_\phi(f_m)}$. This construction avoids the problematic $f_m = 0$. Application of the inverse discrete Fourier transform converts the frequency domain series to a time series representing phase noise values

$$\phi_k = \sum_{m=-M/2}^{M} w_m \sqrt{S_\phi(f_m)} e^{-j2\pi mk/M}. \tag{3.21}$$

Figures 3.5 and 3.6 both show several realizations of phase noise trajectories as a function of time. The time axis is scaled in units of PRI T_r, where $T_r = 8.33$ ms. The observation time is a CPI, $T_{\text{CPI}} = 16T_r = 133.33$ ms. It is noted that all realizations result in approximately linear trajectories over the CPI. In Figure 3.4, the observation time is much longer, and the trajectories are not linear any more. Thus, from empirical observations, during a CPI, the phase noise at a sensor may be modeled by a stochastic process

$$\phi(t) = \alpha t + \psi(t), \tag{3.22}$$

where α is a random variable representing the slope of the phase trajectory and $\psi(t)$ is a stochastic process representing the deviation from the linear term. By construction, and since the w_m in (3.21) are zero mean, the phase noise process is zero mean, $E[\phi(t)] = 0$. The zero-mean property implies that $E[\alpha] = 0$, and $E[\psi(t)] = 0$. For later use, we note that

$$E\left[\phi^2(t)\right] = E\left[\alpha^2\right] t^2 + E\left[\psi^2(t)\right]. \tag{3.23}$$

The phase noise processes are mutually independent betwen sensors.

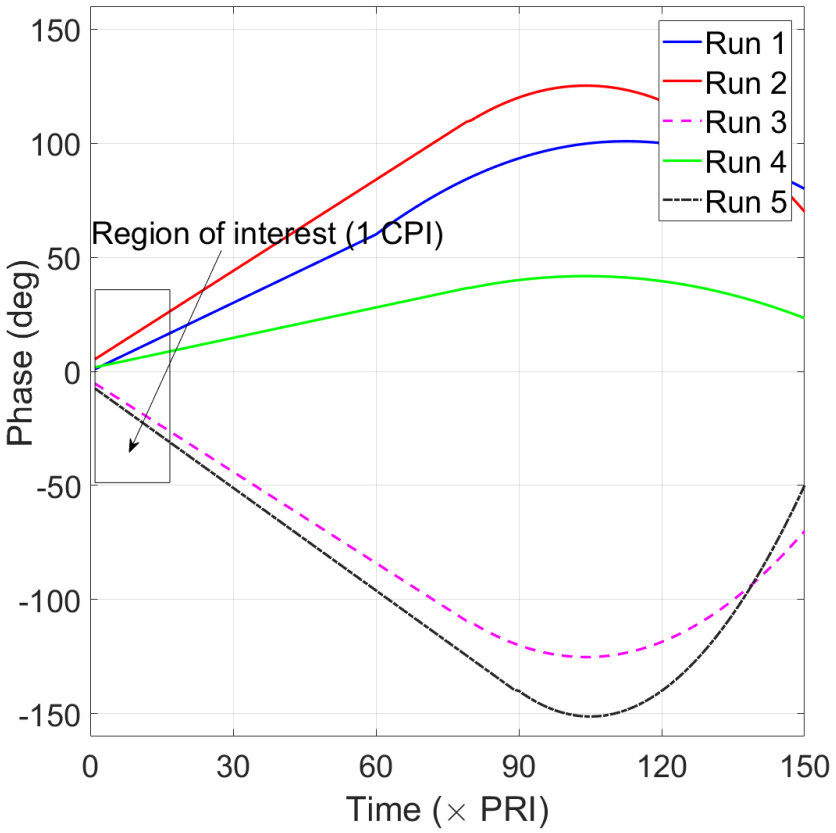

Figure 3.4 Examples of phase trajectories at longer time interval for VCO.

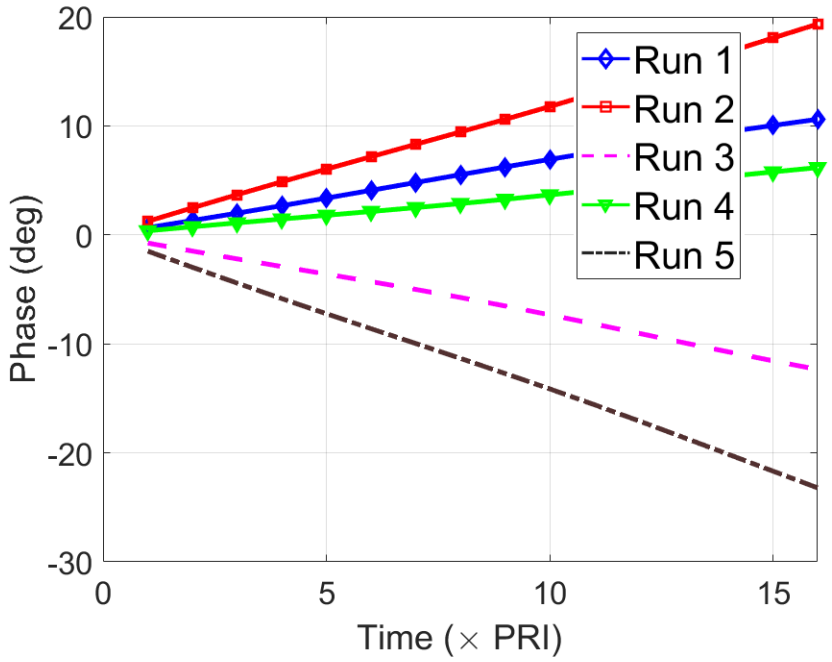

Figure 3.5 Examples of phase trajectories for USO.

The time interval of interest is $T_r \leq t \leq T_{\text{CPI}}$ corresponding to the frequency interval $1/T_{\text{CPI}} \leq f \leq 1/T_r$. For a process $\phi(t)$ with power spectral density $S_\phi(f)$, the variance σ_ϕ^2 is given by

$$\sigma_\phi^2 = \int_{1/T_{\text{CPI}}}^{1/T_r} S_\phi(f) df. \tag{3.24}$$

In the time domain, from (3.23), the variance of $\phi(t)$ is time-dependent. The variance σ_ϕ^2 may also be obtained by averaging $E[\phi^2(t)]$ over the coherent processing interval

$$\sigma_\phi^2 = \frac{1}{T_{\text{CPI}}} \int_0^{T_{\text{CPI}}} E\left[\phi^2(t)\right] dt. \tag{3.25}$$

From the empirical almost linear phase trajectories shown in Figure 3.5 , and to simplify the analysis, assume that $E[\psi^2(t)] \ll E[\alpha^2] t^2$. Then, from (3.23),

$$E\left[\phi^2(t)\right] \approx \sigma_\alpha^2 t^2 \tag{3.26}$$

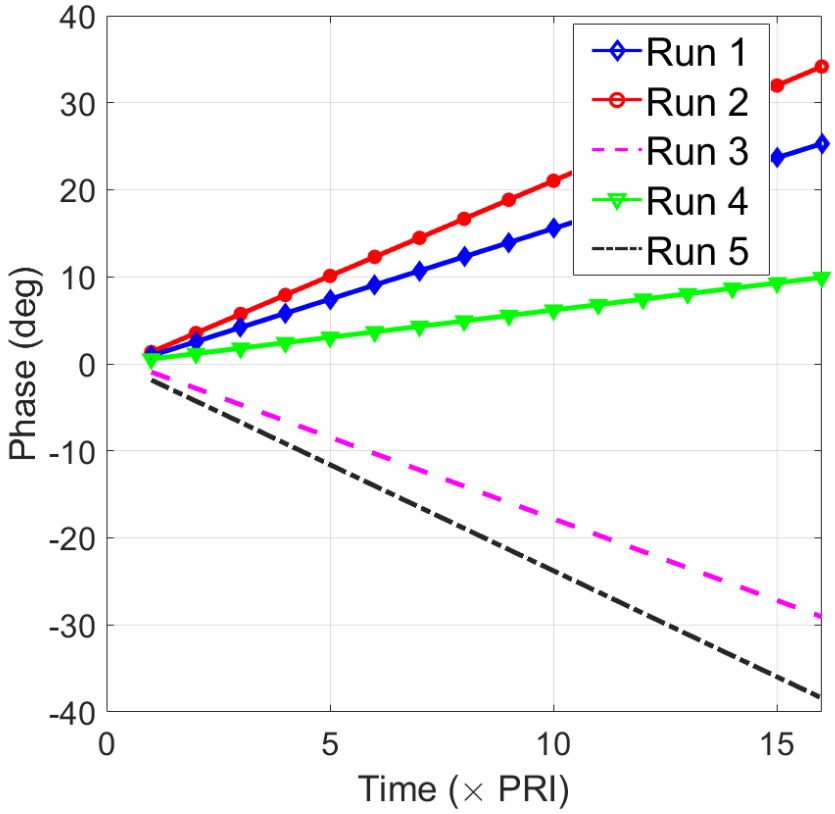

Figure 3.6 Examples of phase trajectories for VCO.

where $\sigma_\alpha^2 = E\left[\alpha^2\right]$. Substituting $E\left[\phi^2\left(t\right)\right]$ from (3.26) into (3.25) and evaluating the integral, we obtain an expression for the average variance of the phase noise over the observation interval

$$\sigma_\phi^2 = \frac{\sigma_\alpha^2 T_{\text{CPI}}^2}{3} \tag{3.27}$$

From this expression, the average variance grows quadratically with the length of the coherent processing interval. Given the average phase noise variance σ_ϕ^2 (3.24), the variance of the slopes of the phase noise trajectory may be computed from

$$\sigma_\alpha^2 = \frac{3\sigma_\phi^2}{T_{\text{CPI}}^2}. \tag{3.28}$$

This relation is applied in the next section to quantify the effect of phase noise on the array beampattern and Doppler response.

3.4 Effect of Phase Noise on Space-Time Adaptive Processing (STAP)

In this section, we will study the effect of phase noise on the distributed STAP system. These phase errors affect a distributed STAP system two ways: (1) cause errors in spatial processing, (2) cause errors in Doppler processing. In this section, the effect of phase noise on spatial processing is evaluated first, followed by an analysis of the effect of phase noise on Doppler processing. This is followed by a discussion on the effect of phase noise on STAP, which combines spatial and Doppler processing.

3.4.1 Effect of Phase Noise on Spatial Processing

Assume an array formed by sensors, each with its own independent local oscillator. Further, assume that at time $t = 0$, the array is perfectly calibrated, meaning that there are no phase errors, and the array factor is given by (3.2). From the previous discussion, the phase noise at the n-th antenna element index is modeled by a stochastic process $\phi_n(t) = \alpha_n t + \psi_n(t)$. The array factor in the presence of phase

noise is a function of time and may be expressed

$$b(u;t) = \frac{1}{N_s}\sum_{n=1}^{N_s} e^{j(k_0 z_n u + \phi_n(t))} \tag{3.29}$$

where t is the time elapsed from calibration. We are interested in the effect of phase noise in the sidelobe region $|u| > 1/Z$, where $|b(u;t)| \ll 1$. Applying the small phase approximation $e^{j\phi_n(t)} \approx 1 + \phi_n(t)$,

$$b(u;t) = \frac{1}{N_s}\sum_{n=1}^{N_s} e^{jk_0 z_n u}\left(1 + j\phi_n(t)\right). \tag{3.30}$$

Since $\phi_n(t)$ are zero-mean and independent between sensors:

$$E\left[b(u;t)\right] = \frac{1}{N_s}\sum_{n=1}^{N_s} e^{j2\pi z_n u} = b_0(u) \tag{3.31}$$

where $b_0(u)$ is the array factor of the ideal array (no phase errors) given by (3.2). The variance of the array factor in the sidelobe region, is a measure of the sidelobes generated by the phase errors between the elements. The variance $\sigma_b^2(u;t)$ of the spatial array factor in the sidelobe region is given by

$$\sigma_b^2(u;t) = E\left[|b(u;t)|^2\right] - \left(b_0(u)\right)^2. \tag{3.32}$$

To compute $\sigma_b^2(u;t)$ substitute (3.30) in (3.32), apply $E\left[\phi(t)\right] = 0$ as discussed previously, and after some manipulations, it can be shown that

$$E\left[|b(u;t)|^2\right] = \frac{1}{N_s}E\left[\phi^2(t)\right] + b_0(u) \tag{3.33}$$

from which it follows that

$$\sigma_b^2(u;t) = \frac{1}{N_s}E\left[|\phi(t)|^2\right]. \tag{3.34}$$

Thus, the variance σ_b^2 of the array pattern is a function of time, but not a function of the angle of arrival of the signal, $\sigma_b^2(u;t) = \sigma_b^2(t)$. An analytical expression for σ_b^2

is obtained from (3.26) and (3.28):

$$\sigma_b^2(t) = \frac{1}{N_s}\sigma_\alpha^2 t^2 = \frac{3\sigma_\phi^2 t^2}{N_s T_{\text{CPI}}^2} \tag{3.35}$$

The significance of this expression is that phase noise produces changes in the sidelobes of the beampattern. The sidelobes due to phase noise are independent of the space variable u, but increase with the time elapsed from phase calibration.

3.4.2 Effect of Phase Noise on Doppler Processing

Assume zero phase errors at time $m = 0$, and let $\phi\left((m-1)T_r\right),\ m = 1, ..., N_p$ represent the phase noise at samples taken at the radar receiver at the pulse repetition frequency $1/T_r$. Modifying (3.7) to account for the presence of phase noise, the Doppler array factor is expressed

$$d\left(f\right) = \frac{1}{N_p}\sum_{m=1}^{N_p} e^{j2\pi f(m-1)T_r + \phi((m-1)T_r)}. \tag{3.36}$$

We are interested in the effect of phase noise on both the mainlobe and sidelobes of the Doppler array factor. For the mainlobe analysis, we apply the approximation $\phi\left((m-1)T_r\right) \approx \alpha\left((m-1)T_r\right)$ (see (3.22)),

$$d\left(f\right) = \frac{1}{N_p}\sum_{m=1}^{N_p} e^{j2\pi f(m-1)T_r + \alpha(m-1)T_r} \tag{3.37}$$

After a little algebra, it can be shown that conditioned on the trajectory slope α, the magnitude of the array factor may be expressed

$$\left|d\left(f\right)\right| = \left|\frac{\sin\left(\left(N_p-1\right)\pi(f+\alpha/2\pi)T_r\right)}{N_p \sin\left(\pi(f+\alpha/2\pi)T_r\right)}\right|. \tag{3.38}$$

Comparing this expression with the ideal case of no phase noise $(\alpha = 0)$,

$$\left|d_0\left(f\right)\right| = \left|\frac{\sin\left(\left(N_p-1\right)\pi f T_r\right)}{N_p \sin\left(\pi f T_r\right)}\right| \tag{3.39}$$

the effect of phase noise is observed to be an offset $\Delta f = -\alpha/(2\pi)$ in the mainlobe.

The sidelobes for the Doppler array factor are in the region $|f| > 1/T_{\text{CPI}}$. Applying the small phase approximation, $e^{j\phi_n((m-1)T_r)} \approx 1 + j\phi((m-1)T_r)$ in (3.36), the array factor is given by

$$d(f) = \frac{1}{N_p} \sum_{m=1}^{N_p} e^{j2\pi f(m-1)T_r} \left(1 + j\phi\left((m-1)T_r\right)\right). \tag{3.40}$$

Since $\phi((m-1)T_r)$ is zero mean, the mean value of the array factor is

$$E\left[d(f)\right] = \frac{1}{N_p} \sum_{m=1}^{N_p} e^{j2\pi f(m-1)T_r} = d_0(f). \tag{3.41}$$

The variance of the Doppler array factor in the sidelobe region, is a measure of the sidelobes generated by the phase errors between the time samples used to estimate Doppler. The variance is given by

$$\sigma_d^2(f) = E\left[|d(f)|^2\right] - \left(d_0(f)\right)^2. \tag{3.42}$$

To compute $\sigma_d^2(f)$ substitute $d(f)$ from (3.40) in (3.42), apply $E\left[\phi\left((m-1)T_r\right)\right] = 0$, and after some manipulations, it can be shown that

$$E\left[|d(f)|^2\right] = \frac{1}{N_p^2} \sum_{m=1}^{N_p} E\left[\phi^2\left((m-1)T_r\right)\right] + d_0(f). \tag{3.43}$$

It follows that

$$\sigma_d^2 = \frac{1}{N_p^2} \sum_{m=1}^{N_p} E\left[|\phi\left((m-1)T_r\right)|^2\right]. \tag{3.44}$$

The last expression is not a function of the frequency f, which implies that the variance of the Doppler array pattern is constant across the sidelobes. An analytical expression for σ_d^2 is obtained by approximating the integral in (3.25) with the sum in

(3.44):

$$\begin{aligned}\sigma_\phi^2 &= \frac{1}{T_{\text{CPI}}}\int_0^{T_{\text{CPI}}} E\left[\phi^2(t)\right] dt \\ &\approx \frac{1}{T_{\text{CPI}}}\sum_{m=1}^{N_p} E\left[\left|\phi\left((m-1)T_r\right)\right|^2\right] T_r \\ &= \frac{1}{N_p}\sum_{m=1}^{N_p} E\left[\left|\phi\left((m-1)T_r\right)\right|^2\right]. \end{aligned} \tag{3.45}$$

Comparing (3.44) and (3.45), it follows that

$$\sigma_\phi^2 = N_p\sigma_d^2 \tag{3.46}$$

Finally, substituting (3.27) and since $T_{\text{CPI}} = N_pT_r$.

$$\sigma_d^2 = \frac{\sigma_\phi^2}{N_p} = \frac{N_p\sigma_\alpha^2 T_r^2}{3} \tag{3.47}$$

The sidelobe variance increases linearly with the number of pulses used for Doppler processing and quadratically with the pulse repetition interval.

3.5 Effect of Phase Noise on STAP

As discussed in the previous subsections, phase noise affects STAP via multiple mechanisms. First, phase errors between independent oscillators affect spatial processing, second, phase errors accumulate as a function of time, and interfere with Doppler processing. In particular, low frequency components of phase noise cause an offset in the mainlobe of the Doppler array factor. In this subsection, the effect of phase noise on target detection is demonstrated by numerical examples of the clutter rank, the signal to noise and interference ratio (SINR) and receiver operating characteristics (ROC). The analysis assumes ideally calibrated sensors at time $t = 0$.

The clutter covariance matrix quantifies the correlation between all pairs of space-time measurements due to reflections from ground clutter. The rank of the

clutter covariance matrix determines the amount of data required to train an adaptive processor as well as the overall detection performance of the system. Accurate clutter rank estimation is important for the design of computationally feasible, reduced-rank adaptive processing algorithms. Therefore, characterization of clutter rank is an important step for understanding STAP performance. Clutter rank is well understood for uniform, linear arrays aligned along the radar platform velocity vector. The equation that governs this case is called Brennan rule [6], [7]. The clutter rank observed by arbitrary arrays, however, is not as well understood.

Doppler processing discriminates targets that have radial velocity relative to the antenna elements. Clutter from direction perpedincular to the flight path appears stationary since it has zero radial velocity. The challenge in GMTI is that clutter in directions other than perpendicular to the flight path has non-zero Doppler shifts. These clutter returns may hinder the detection of slow-moving targets. SINR as a function of Doppler shift is a useful metric for estimating the minimum detectable velocity (MDV) at which a target may be discriminated from the clutter.

In this section, numerical results are presented for a filled uniform linear array (ULA) with $N_s = 20$ elements and $N_p = 16$ time samples. Antenna elements are assumed to operate with autonomous oscillators. The signal to noise ratio SNR = 15 dB and the clutter to noise ratio CNR = 30 dB. The covariance matrix used to obtain the numerical results is the theoretical covariance matrix (3.10). The clutter covariance matrix was computed from a numerical approximation to (3.11). Given the covariance matrix $\mathbf{R}$, the SINR was computed from the expression

$$\text{SINR}(u, f) = \mathbf{a}^H(u, f)\mathbf{R}^{-1}\mathbf{a}(u, f). \tag{3.48}$$

Figure 3.7 shows the effect of phase noise on the clutter rank for the two examples of oscillators considered in this work. STAP relies on the fact that the rank of the clutter covariance matrix $\mathbf{R}_c$ is much lower than the dimensionality of

the signal space. In this case, whitening of the clutter interference does not result in significant loss of target SNR. In a filled ULA, the clutter map (defined as the plot of $\mathbf{a}^H(u,f)\mathbf{R}_c\mathbf{a}(u,f)$ obtained by u and v sweeping through their domains $|u| < 1$, $|fT_r| < 0.5$), forms a diagonal ridge in the u-f plane. The clutter rank is a measure of the area in u-f space covered by the clutter ridge. A lower clutter rank generally implies better STAP performance. The clutter rank shown in Figure 3.7 is an average of 150 simulation runs. An increase in the clutter rank is observed when phase noise affects the operation of the array. The increase in clutter rank is larger for the VCO, which has larger phase noise.

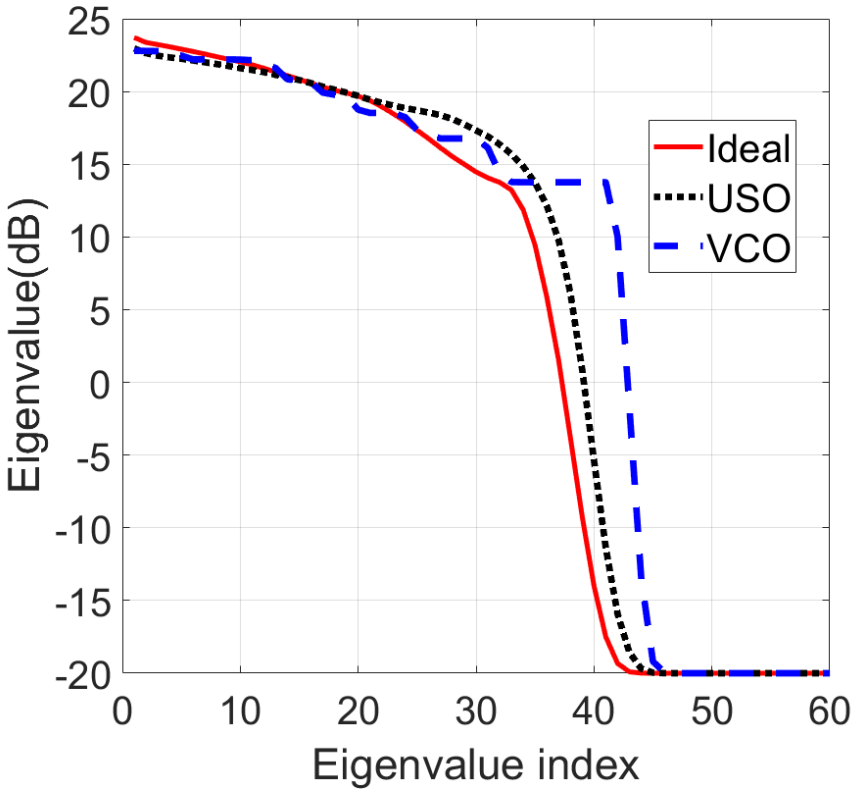

Figure 3.7 Effect of phase noise on clutter rank.

Figure 3.8 demonstrates the effect of phase noise on the signal to interference and noise ratio (SINR) of STAP with USO and VCO. From Figure 3.8 it is observed

that the MDV is with phase noise is similar to the ideal case, but the maximum SINR degrades with the phase noise, with the degradation being higher for the VCO.

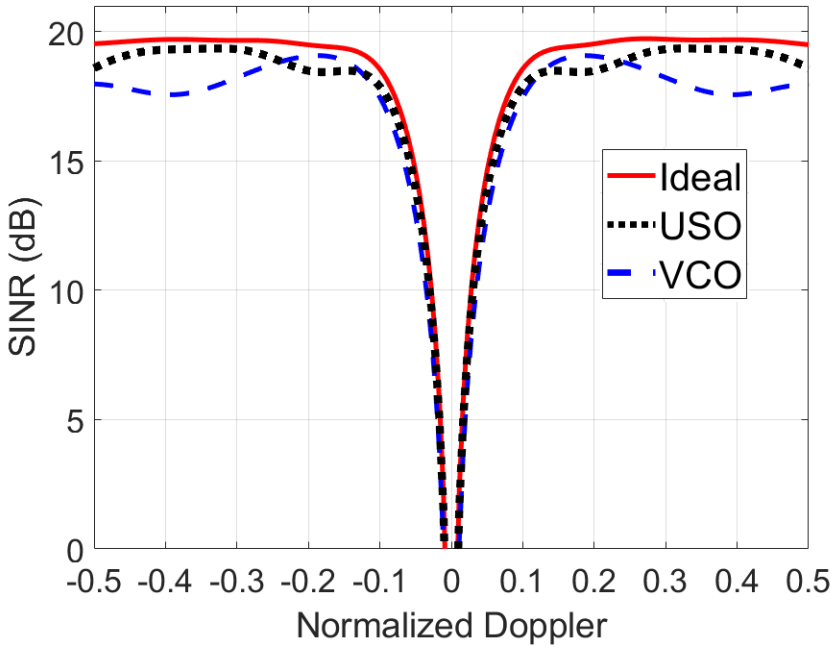

Figure 3.8 Effect of phase noise on SINR.

Figure 3.9 shows the effect of phase noise on the ROC of a STAP system implemented as a distributed array. The ROCs shown are averaged over 100 runs. Phase noise reduces detection performance, but an array equipped with USOs has better performance than array equipped with VCOs.

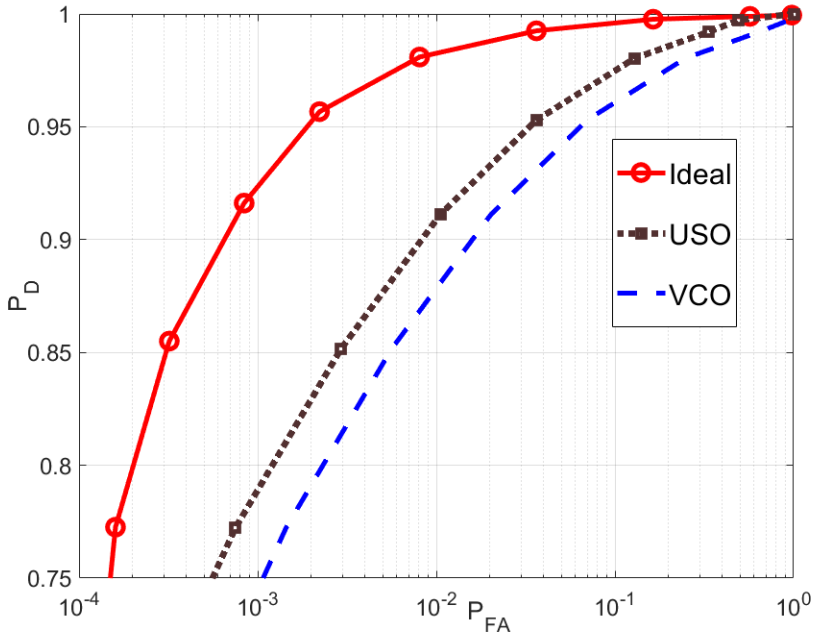

Figure 3.9 Effect of phase noise on ROC.

CHAPTER 4

IMPAIRMENTS IN DISTRIBUTED STAP AND PROPOSED METHOD FOR SYNCHRONIZATION AND CALIBRATION

In this chapter the effects on STAP performance of various errors stemming from the distributed architecture: frequency offsets, generalized motion, sparse aperture, and sensor location errors are evaluated . Performance is first evaluated subject to each type of impairment assuming ideal conditions with respect to the other impairments. The combined effect of all impairments, including phase noise, is also evaluated. The performance metrics for individual impairments are the clutter rank and SINR, while the combined effect of all impairments is also measured by ROCs. The second part of this chapter outlines a technique for phase and sensor location calibration for distributed STAP system. We presented a STAP calibration algorithm, followed by the numerical results. Unless specified otherwise, the parameters used for the simulations are the same as in Chapter 3.

4.1 Frequency Offset

In the previous chapter the effect of phase noise on STAP was discussed. In addition to phase noise, distributed sensors, each equipped with its own oscillator, are subject to frequency offset errors. Even though all sensors are instructed to tune to the same frequency, the carrier frequency of a sensor would typically have some error (offset) relative to the nominal frequency setting. The frequency offset is in addition to the effect of phase noise, but its effect is first evaluated assuming oscillators without phase noise.

Figure 4.1 shows the effect of frequency offset on the clutter rank (left panel) and SINR (right panel) of a distributed STAP system with parameters specified in Section IV.C. Two levels of frequency offsets typical to commercial oscillators were

evaluated, 0.1 ppm and 0.5 ppm. Figure 4.1 shown are averages of 150 runs. A slight increase is observed in the clutter rank, with the higher clutter rank corresponding to the larger higher frequency offset. The SINR curve shows a degradation of 2-4 dB in SINR, but no visible effect on the MDV.

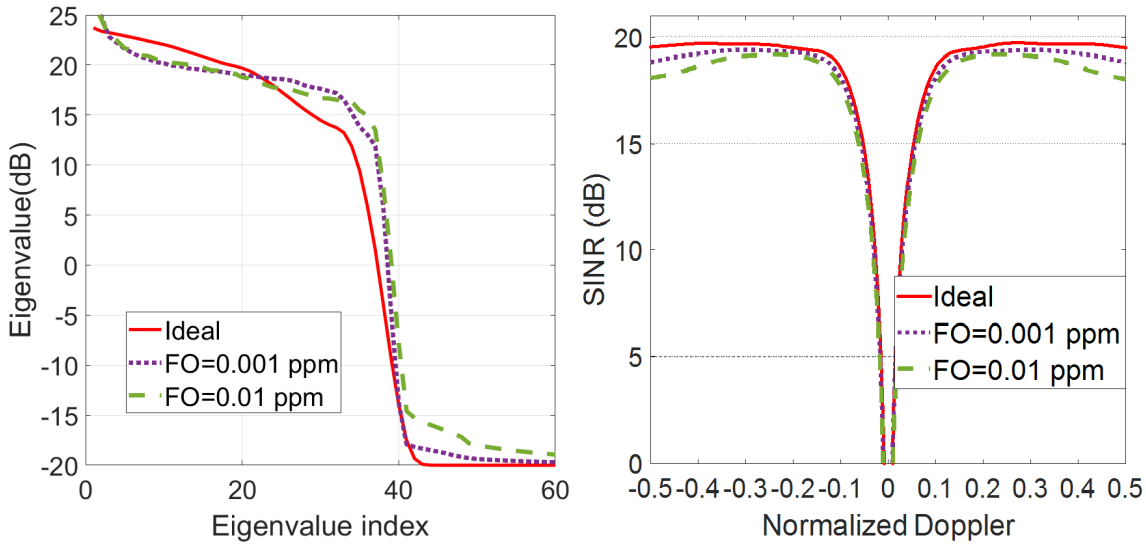

Figure 4.1 Effect of frequency offset on clutter rank (left) and SINR (right).

4.2 Generalized Motion

In this performance evaluation, the radar sensors' local oscillators are assumed perfectly synchronized in phase and frequency, but each sensor moves independently in terms of speed and direction. For convenience, it is assumed that during the CPI of interest, and the independent motion parameters notwithstanding, the sensors form a ULA. The motion parameters for an arbitray sensor and target are shown in Figure 3.1. The origin of the coordinate system is arbitrarily located at the first sensor, and the horizontal axis of the coordinate system is colinear with the array. Numerical examples are shown for two sets of motion parameters. In the first case, each sensor has a velocity chosen from a uniform distribution in the range 50 to 70 m/s and a direction chosen from a uniform distribution with the range $\pm\pi/10$ radians. In the

second case, each sensor has a velocity chosen from a uniform distribution in the range 40 to 80 m/s and a direction chosen from a uniform distribution with the range $\pm\pi/5$ radians. Figures shown are averages of 150 runs.

Figure 4.2 shows the effect of individual sensor motion on clutter rank (left panel) and SINR (right panel). The figure indicates an increse in clutter rank and a decrease in SINR for the generalized motion cases. The higher the variation between motion parameters of sensors, the larger the change in clutter rank and SINR relative to the ideal case in which all sensors have the same motion parameters.

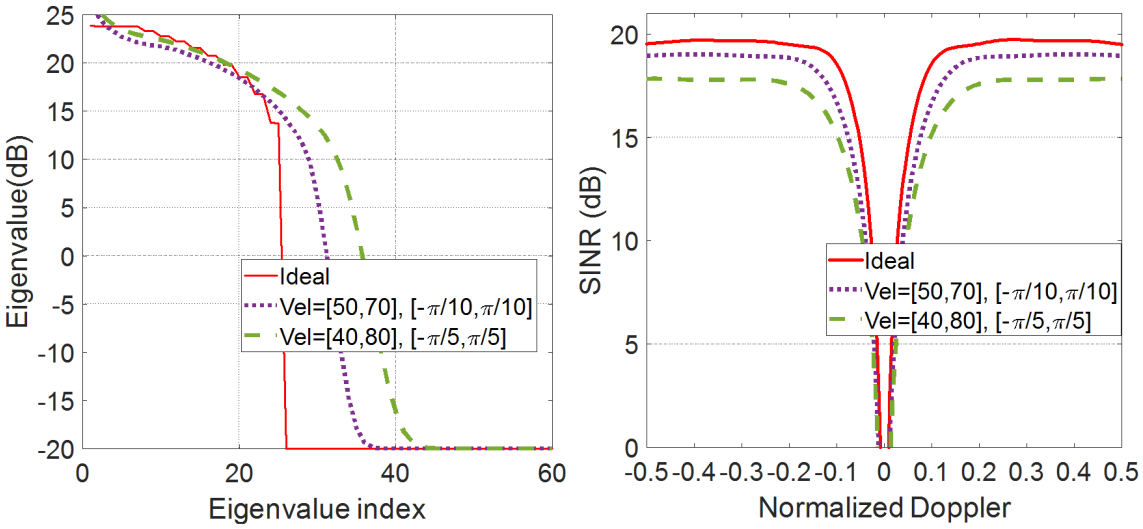

Figure 4.2 Effect of sensors moving autonomously on clutter rank (left) and SINR (right).

4.3 Large Aperture Random Array

The numerical results presented sofar were obtained assuming a ULA. In a distributed system, sensors are likely to be spaced irregulary and intervals larger than $\lambda/2$. Large aperture, but sparse element-wise arrays are known in the literature as random arrays [61] [62]. The beamwidth of a linear random array is determined by the aperture length, while average and peak sidelobes are controlled by the number of elements in

the array. The spatial array factor $b_0(u)$ (3.2) may be viewed as a stochastic process, where the element locations z_n are random variables. The properties of such random arrays were analyzed in [61], [62], while the performance of random arrays in STAP has been analyzed in [63].

All the arrays analyzed in this section have $N_s = 20$ elements. A 20-element ULA has a 10λ aperture. Random arrays analyzed had apertures 50λ and 100λ. Note that a 100λ array with 20 elements has only 1/10 of the number of elements of a 100λ ULA. For each of the 150 runs, the location of two elements was set at each end of the array, while the locations of the other 18 elements was chosen randomly from a uniform distribution with range 100λ. Figure 4.3 shows the effect of random, sparse arrays on clutter rank (left panel) and SINR (right panel). The clutter rank increases significantly since it is determined by the number of elements in a filled array. Thus the clutter rank of the 100λ random array is the same as that of a 100λ ULA. For example, the clutter rank for the STAP system shown in the figure is $N_s' + N_p - 1 = 100 + 16 - 1 = 115$, where N_s' is the number of elements in a 100λ ULA. The significantly more degrees of freedom engaged in clutter cancellation are expected to lower the SINR. This is confirmed by the SINR plot, which shows SINR losses between 2 and 10 dB. On the positive side, a larger aperture is expected to produce a narrower beam, which in turn leads to a reduction in MDV. This is confirmed by the figure.

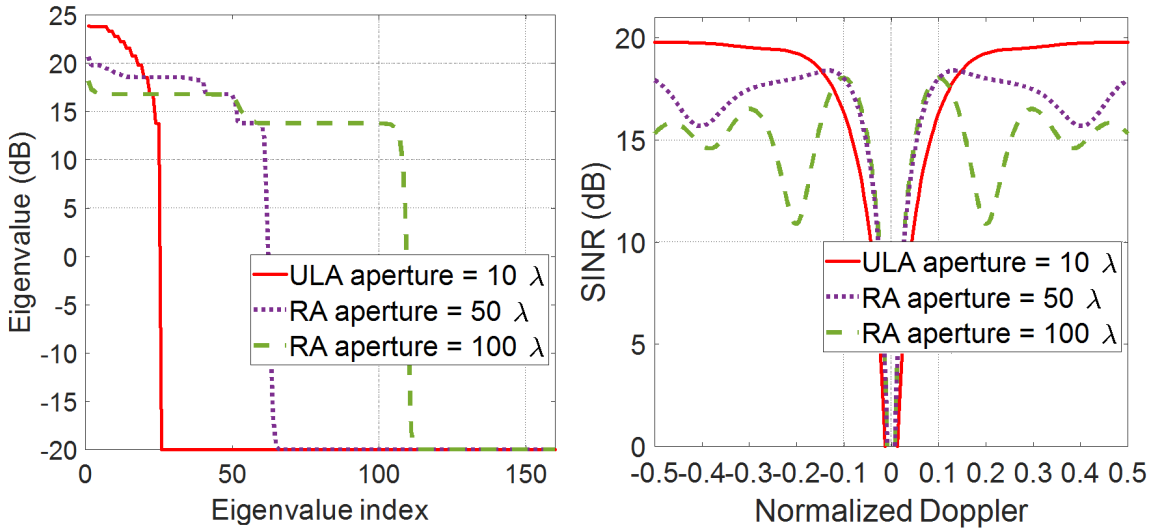

Figure 4.3 Effect of aperture size for a fixed number of array elements $N_s = 20$ on clutter rank (left) and SINR (right).

4.4 Sensor Location Errors

As discussed previously, a typical implementation of distributed STAP entails a large, sparse array. Unlike an array mounted on a single platform, which may be manufactured as one unit with high precision spacing between the elements, in a distributed architecture sensor locations will be known with finite accuracy. In this part is investigated the effect of sensor location errors on STAP performance. Sensor location errors are specified according to the standard deviation of the error assuming a uniform distribution. The effects of two levels of sensor location errors were studied: λ and 2λ. For each case, the location of each sensor of a filled ULA was offset by a random amount.

Figure 4.4 shows effect of array sensor location errors on on clutter rank (left panel) and SINR (right panel). From the figure is observed a slight increase in clutter rank, made larger for the larger location errors. Similarly there is a slight loss of SINR, made larger for larger sensor location errors.

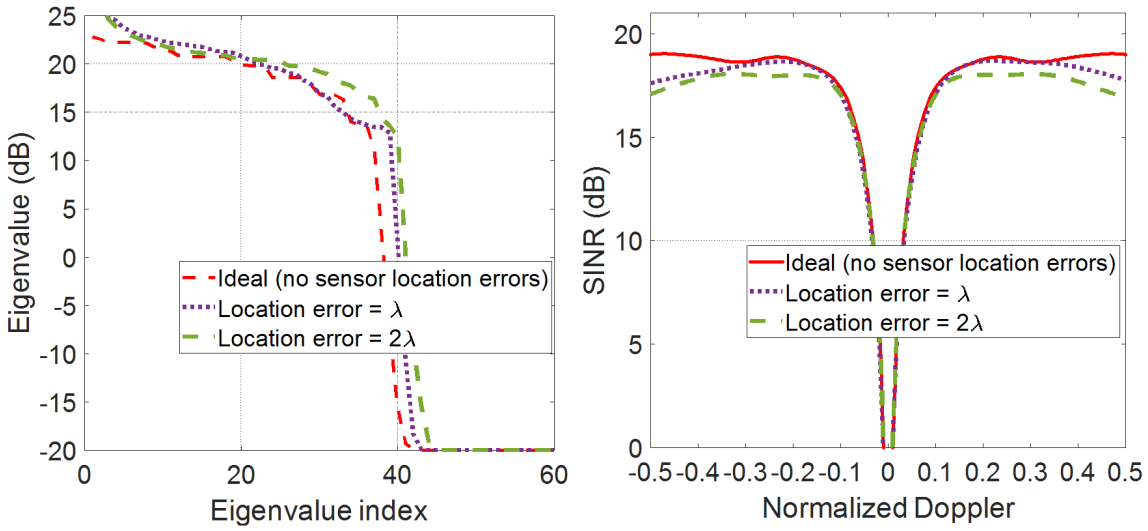

Figure 4.4 Effect of sensor location errors on clutter rank (left) and SINR (right).

4.5 Combined Effect of Impairments

The combined effects on STAP performance of various errors stemming from the distributed architecture: frequency offsets, generalized motion, sparse aperture, and sensor location errors are analyzed in this section. We compared the ideal case, with phase noise only, and with phase noise and other impairments studied in this section for distributed STAP system. The array analyzed in this section contained $N_s = 20$ elements. The level of frequency offsets were evaluated at 0.5 ppm, corresponding to typical commercial oscillators. Figures shown were averages of 150 runs. Each sensor has a velocity chosen from a uniform distribution in the range 40 to 80 m/s and a direction chosen from a uniform distribution with the range $\pm\pi/5$ radians. The sensor location errors were set at 2λ.

Figure 4.5 shows the clutter rank illustrating combined effects of PN, FO, random array, motion, location. From the figure is observed a noticeable increase in clutter rank, made larger for the case of combined errors.

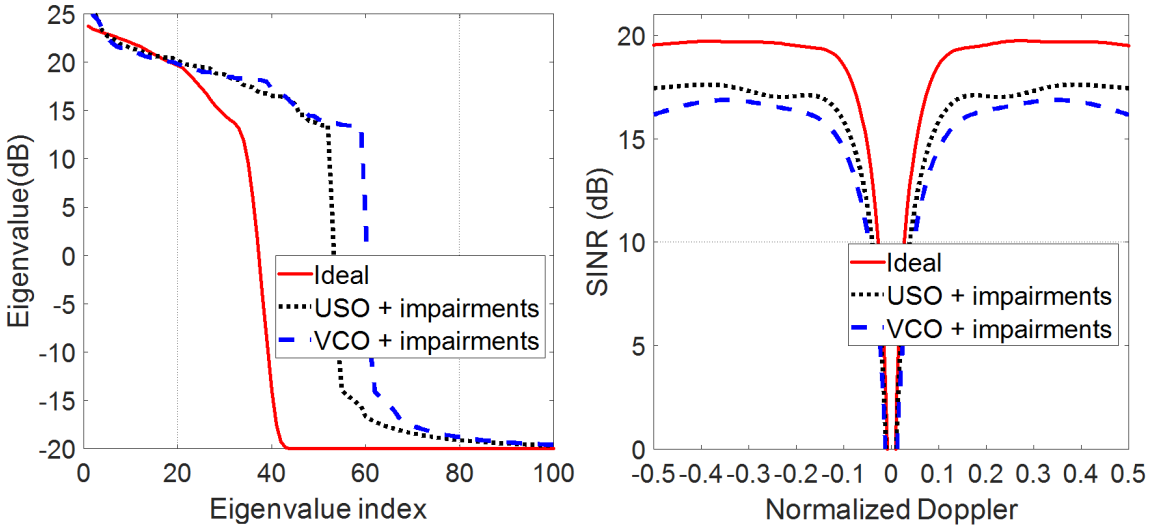

Figure 4.5 Effect of combined effect of impairments on clutter rank (top) and SINR (bottom)

Figure 4.6 shows the effect on ROC curve for $SNR = 15$ dB of the combined effect of impairments. Similarly there is a significant loss of SINR, made larger for larger combined errors.

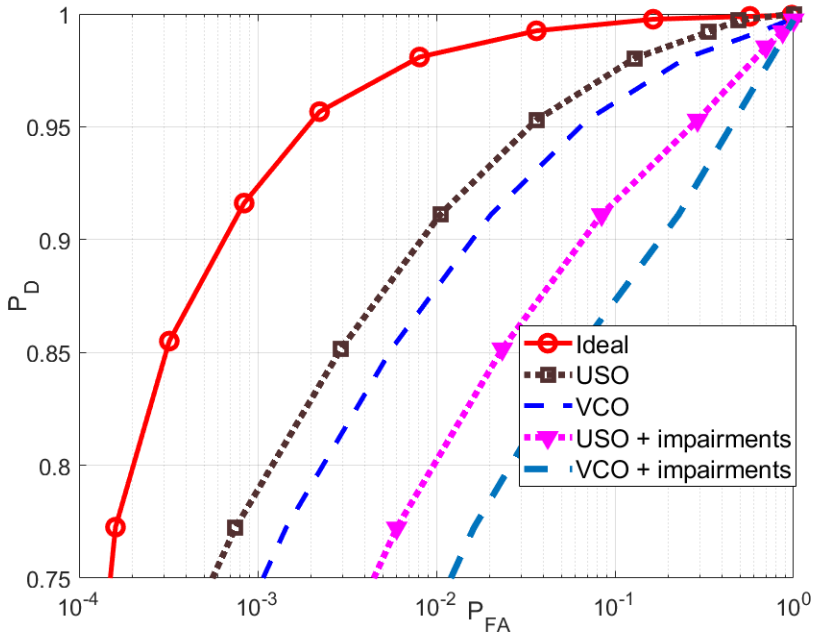

Figure 4.6 Combined effect of impairments on ROC

4.6 Synchronization and Calibration for Distributed STAP

In the previous sections, we consider certain aspects of a distributed implementation of STAP. It has been shown that one of the main challenges of a distributed implementation is that each sensor has its own local oscillator, unlike a traditional array in which all sensors are connected to the same local oscillator. Even when tuned to the same frequency, phase errors between the sensors will develop over time, due to phase instabilities. Hence phase synchronization, or phase noise calibration, needs to be done on the distributed STAP system. Besides, other aspects of synchronization, for example time synchronization, frequency synchronization or frequency offset calibration, sensor location and sensor velocity calibration are also of important to be considered when these oscillators are let run freely.

Figure 4.7 shows the synchronization and calibration architecture for distributed STAP system. We assume the distributed platforms carry out location and phase calibration with the aides from airborne command center, ground command center

(which can be cell tower or radio transmitter tower), ground calibration targets (for example, illuminators or corner reflectors on the ground), and even ground clutter.

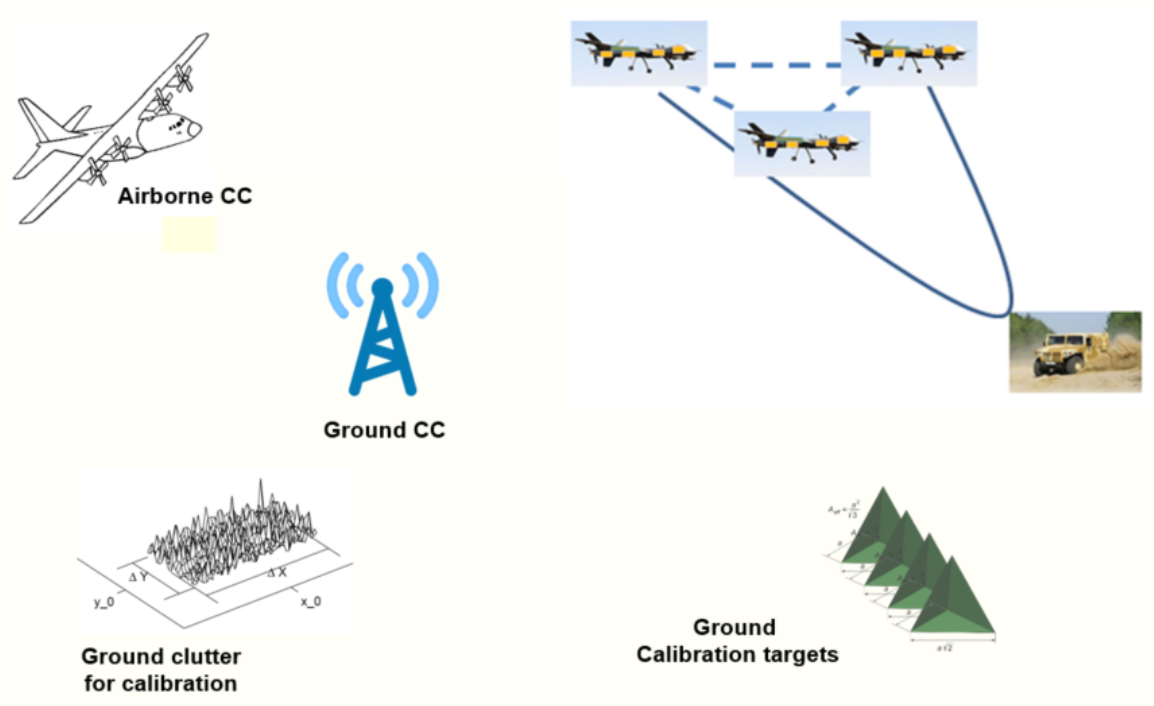

Figure 4.7 Synchronization and Calibration Architectures

There are several papers spanning over the past years discussing certain aspects of distributed radar system and calibration techniques. In [64], the authors describes ground-based distributed coherent aperture system. In [65], Abari et. al. presents AirShare, a primitive that provides ground-based distributed coherent transmission for MIMO radar system. Other works, for example [66], Brown describes a distributed coherent transmission scheme for communication systems and Yang [67] proposes a ground-based wideband distributed coherent aperture radar. To the best of our knowledge, there has not been any work done on calibration of STAP system. In our proposed synchronization architecture, the pilot or reference signals are exploited from the following sources: (1) Ground based command center; (2) Airborne command center; and (3) Measurements subject to Doppler shifts due to ground clutter. In the previous standard documentation, the LTE requirements are base station frequency

accuracy within +/- 0.01 ppm, User equipment frequency accuracy +/- 0.1 ppm, frequency synchronization accuracy within $16 - 50$ ppb. It has been also noted that these requirements are stringent for a communication systems. For a radar system, there has not been any specific guidelines on these calibration values.

Figure 4.8 shows the system model for phase and sensor location calibration of a distributed STAP system. We assume perfect frequency offset and time calibration. The calibration system is based on ground targets at nominally known locations and this technique is built on random array calibration work from [68]. In this radar array system, there consists of a transmitter and N receive sensors. Targets may be present in the far field to the array. Reference targets are targets intentionally placed in the field of view, whose angles of arrival are known nominally. The goal of the system is to detect targets at unknown locations moving with unknown velocities. The radar coordinate system is arbitrarily assumed to be collocated with the transmitter. The locations of the receive sensors are known only approximately. Moreover, the receive sensors are not phase synchronized among themselves or to the transmitter. To detect targets, the system needs to rely on phase synchronized sensors and known sensor locations. Our objective is to develop a method that detects targets based on their angle of arrival and velocity, while at the same time resolves the system unknowns (phase synchronization, accurate sensors locations and accurate reference target locations).

It can be shown that the phase synchronization and sensor location estimation can be solved by a least-squares approach. The main challenge is that phase measurements at each sensor include an unknown number of cycles. The number of cycles cannot be measured directly, but impacts the estimation of the sensors location, and subsequently impacts the localization of unknown targets. The number of cycles depends on the locations of the sensors. The exact locations of the sensors are also unknown, but based on information available a priori, it is possible to determine

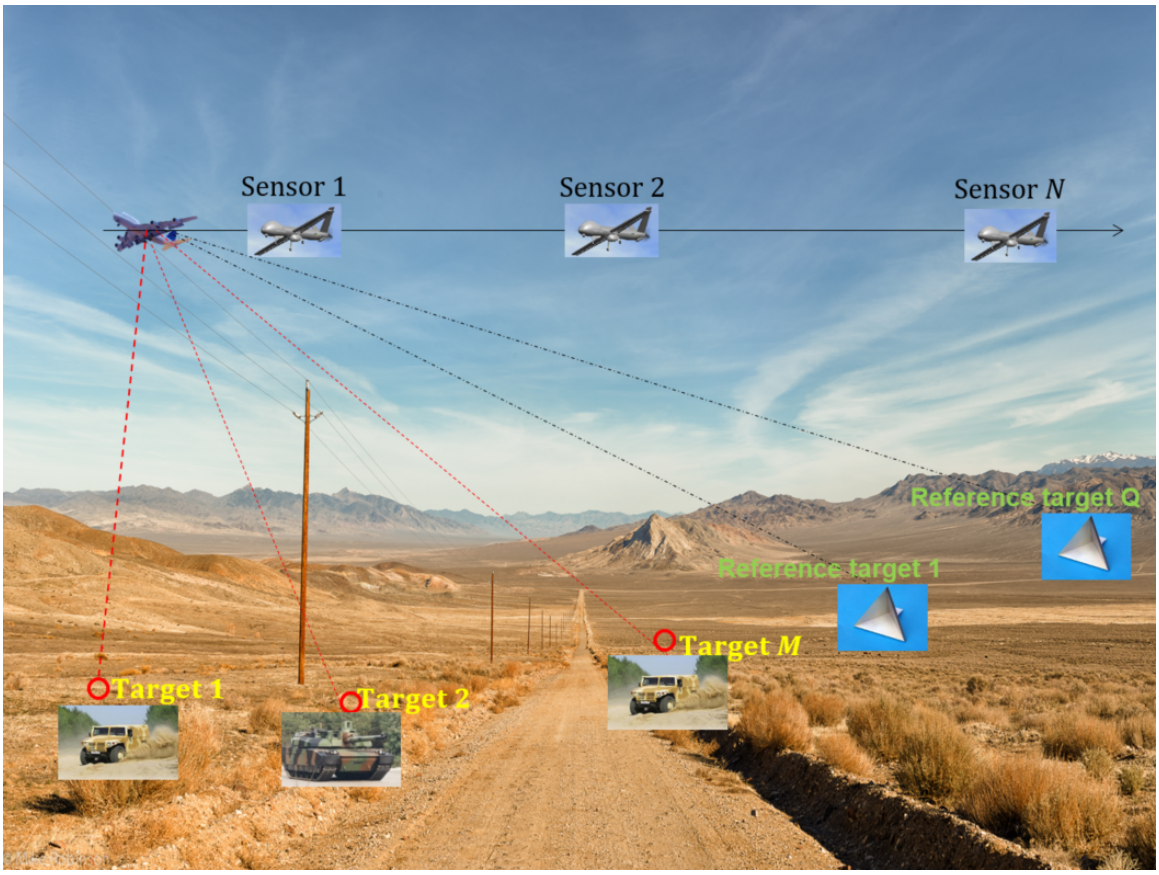

Figure 4.8 Phase and sensor location calibration system model.

a range of possible number of cycles associated with the phase measured at each sensor. Then using these estimations of sensor locations, we subsequently perform targets localization using Matching Pursuit (MP).

Figure 4.9 lists an algorithm to jointly estimate sensors locations and phases information.

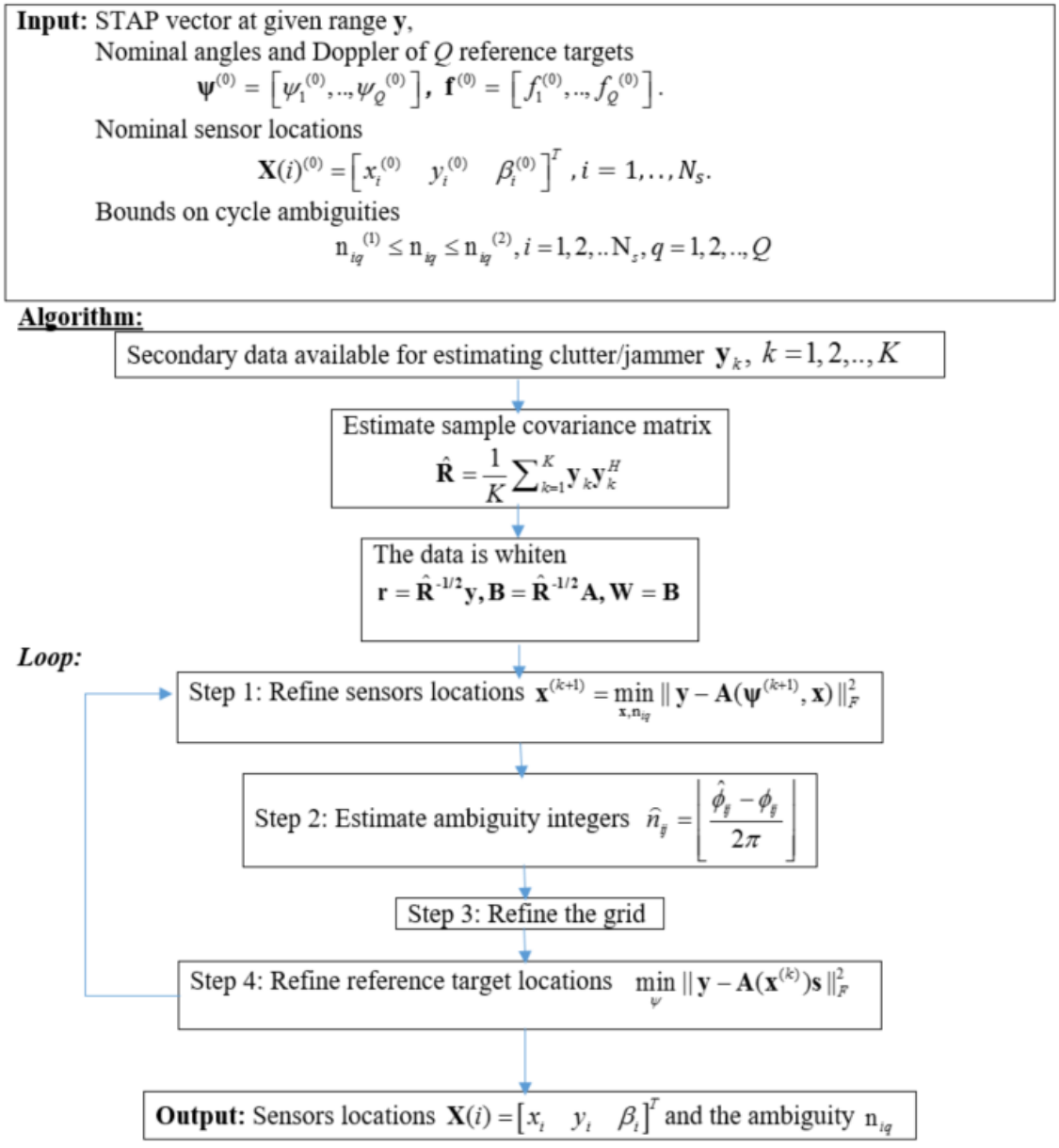

Figure 4.9 STAP calibration algorithm.

Next, numerical results are presented for a distributed array with $N_s = 10$ elements and $N_p = 16$ time samples. Antenna elements are assumed to operate with autonomous oscillators. The signal to noise ratio SNR = 15 dB and the clutter to noise ratio CNR = 30 dB. The covariance matrix used to obtain the numerical results is the theoretical covariance matrix (3.10). The clutter covariance matrix was computed from a numerical approximation to (3.11).

Figure 4.10 shows the receiver operating curve for target detection using three methods: (1) STAP under ideal conditions of known sensor locations and no phase errors, (2) STAP under non-ideal conditions with phase errors, (3) the proposed approach including calibration and detection by MP. It is observed from Figure 4.10 that without calibration, STAP detection experiences a high false alarm rate and low detection probability. Applying the proposed method for phase calibration and target detection improves detection performance dramatically placing it only slightly below the ideal case. For example, with calibration and MP detection, the probability of detection is about 0.9 at a false alarm probability of 10^{-3}.

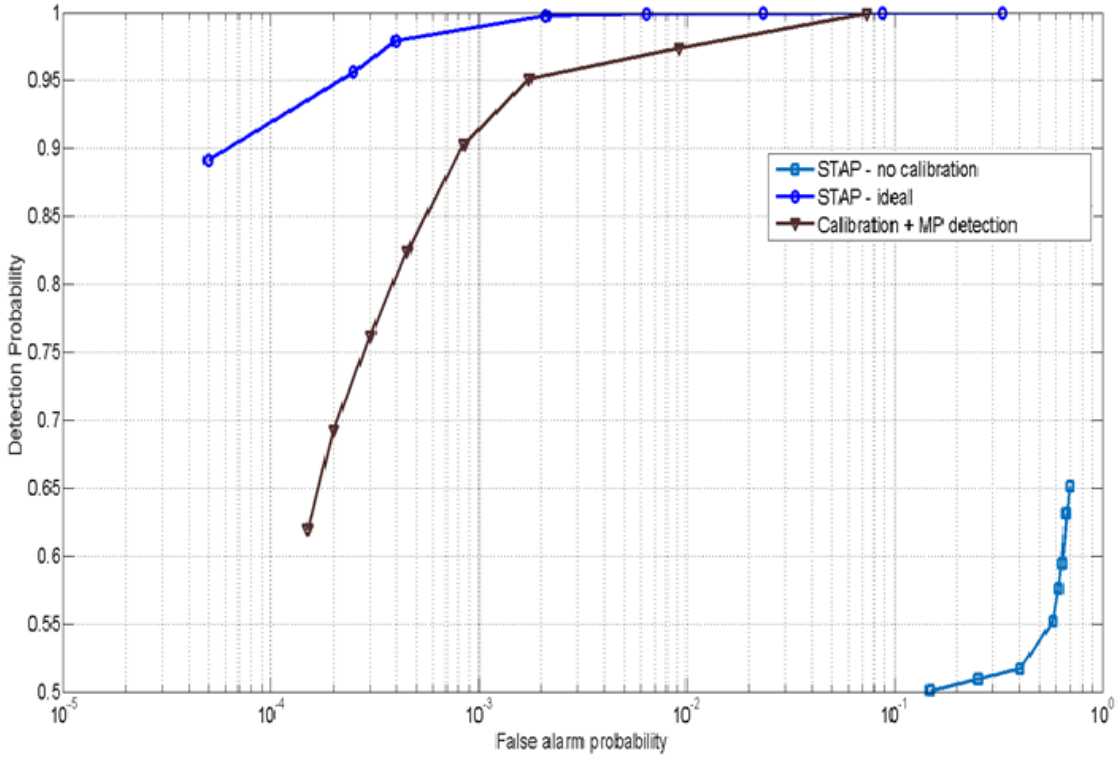

Figure 4.10 STAP calibration algorithm.

4.7 Concluding Remarks

In this chapter, we study the effect of phase noise and other impairments on clutter rank, SINR and receiver operating characteristics. Performance of distributed STAP with respect to system aspects and impairments specific to a coherent distributed system is also analyzed. It is shown that a composite power law model with several terms is required to properly model the phase noise. Simulation results illustrate the effect of phase noise on degrading the performance of target detection using spatial and Doppler processing. Given that phase noise reduces detection performance, an array equipped with USOs exhibits better performance than an array equipped with VCOs. The combined effects on STAP performance stemming from the distributed architecture: frequency offsets, generalized motion, sparse aperture, and sensor location errors are also analyzed. Simulation results illustrate the effect of individual impairment and combined errors on degrading the performance of target detection.

Synchronization and calibration of distributed airborne system present challenging problems that need to be addressed.

CHAPTER 5

CONCLUSIONS

In this dissertation, we propose an approach radically different than STAP, in which sensors are assumed to maintain global time synchronization (e.g. through GPS), but are not phase synchronized. For example, the proposed method would be suitable for implementation by widely distributed, independently moving UAVs, each with its own free-running local oscillator. To support Doppler processing, the oscillator at each sensor is assumed to maintain coherency over the observation time interval, but unlike a phased array, local oscillators are not phase synchronized to each other. To distinguish it from conventional STAP, we refer to the proposed method as distributed STAP. With a system that consists of simple, opportunistic sensors, the processing load is shifted to a fusion center equipped with powerful processing capabilities.

In Chapter 2, we propose a tracker based on the extended Kalman filter that tracks multiple targets based on an observation model in which radar observations are non-linear functions of the targets' states. We refer to this tracker as direct, since it achieves tracking directly from radar observations, rather than from time delays and Doppler shifts. Bayesian Cramer-Rao bound (BCRB) sets the performance limits on target tracking, providing useful tools for evaluating the effect of system parameters on estimation accuracies. In this new approach the multiple moving target tracking problem in MIMO radar systems can be solved. Based on this study, two tracking schemes are proposed. The first is an indirect tracking approach, based on time delay and velocity estimates and implicit nearest-neighbor data association at the fusion center. The second is a direct scheme, based on radar observations tracking and the data association of multiple targets is implicit. The later eliminates intermediate estimated parameters and tracks the moving targets with higher accuracy. Numerical

results show that for multiple targets, direct tracking algorithm outperforms indirect tracking at all SNR values.

In Chapter 3, we study the effect of phase noise and other impairments on STAP with distributed antenna arrays. We envision a STAP application, in which spatial and Doppler processing are performed over a coherent processing interval. We demonstrate that a power law phase noise PSD model is suitable for analyzing the distributed radar system. Then we propose a simplified time-domain model for the phase noise, develop analytical expressions that quantify the effect of phase noise on the array beampattern as a function of time, and propose a generalized motion model for distributed STAP system. It is demonstrated that the effect of phase noise and other impairments on target detection by numerical examples of receiver operating characteristics (ROC).

The main focus of this work was on the development of a distributed architecture for GMTI radar. We study the effect of phase noise and other impairments on clutter rank, SINR and receiver operating characteristics. Performance of distributed STAP with respect to system aspects and impairments specific to a coherent distributed system is also analyzed. It is shown that a composite power law model with several terms is required to properly model the phase noise. Simulation results illustrate the effect of phase noise on degrading the performance of target detection using spatial and Doppler processing. Given that phase noise reduces detection performance, an array equipped with USOs exhibits better performance than an array equipped with VCOs. The combined effects on STAP performance stemming from the distributed architecture: frequency offsets, generalized motion, sparse aperture, and sensor location errors are also analyzed. Simulation results illustrate the effect of individual impairment and combined errors on degrading the performance of target detection.

BIBLIOGRAPHY

[1] M. C. Wicks, "Radar the next generation-sensors as robots," in *Radar Conference, 2003. Proceedings of the International*. IEEE, 2003, pp. 8–14.

[2] W. DeBusk, "Unmanned aerial vehicle systems for disaster relief: Tornado alley," in *AIAA Infotech@ Aerospace 2010*, p. 3506.

[3] A. K. Mitra, "Position-adaptive uav radar for urban environments," in *Radar Conference, 2003. Proceedings of the International*. IEEE, 2003, pp. 303–308.

[4] C. E. Schwartz and J. Noonan, "A radar for unmanned air vehicles," *EURASIP Journal on Applied Signal Processing*, vol. 2005, pp. 37–49, Jan. 2005.

[5] R. L. Moses, L. C. Potter, and M. Cetin, "Wide-angle sar imaging," in *Algorithms for Synthetic Aperture Radar Imagery XI*, vol. 5427. International Society for Optics and Photonics, 2004, pp. 164–176.

[6] M. Weiß, O. Peters, and J. Ender, "First flight trials with artino," in *Synthetic Aperture Radar (EUSAR), 2008 7th European Conference on*. VDE, 2008, pp. 1–4.

[7] R. Klemm, "Adaptive clutter suppression for airborne phased array radars," *Microwaves, Optics and Antennas, IEE Proceedings H*, vol. 130, pp. 125–132, Feb. 1983.

[8] T. J. Nohara, P. Weber, A. Premji, and T. Bhattacharya, "Airborne ground moving target indication using non-side-looking antennas," in *IEEE Radar Conf.*, Dallas, TX, 1998, pp. 269–274.

[9] J. N. Entzminger, C. A. Fowler, and W. J. Kenneally, "Jointstars and GMTI: Past, present and future," *IEEE Trans. on Aerospace and Electron. Syst.*, vol. 35, no. 2, pp. 748–761, Apr. 1999.

[10] P. M. Corbell, J. J. Perez, and M. Rangaswamy, "Enhancing GMTI performance in non-stationary clutter using 3d STAP," in *Proc. IEEE Radar Conf.*, Boston, MA, 2007, pp. 647–652.

[11] D. J. Rabideau and S. M. Kogon, "A signal processing architecture for space-based GMTI radar," in *Proc. Radar Conf.*, Waltham, MA, Apr. 1999, pp. 96–101.

[12] L. E. Brennan and L. Reed, "Theory of adaptive radar," *IEEE Trans. on Aerospace and Electron. Syst.*, vol. AES-9, no. 2, pp. 237–252, Mar. 1973.

[13] J. Ward, "Space-time adaptive processing with sparse antenna arrays," in *Proc. 32nd Asilomar Conf. on Signals, Syst., and Comput.*, Pacific Grove, CA, Nov. 1998, pp. 1537–1541.

[14] T. K. Sarkar, H. Wang, S. Park, R. Adve, J. Koh, K. Kim, Y. Zhang, M. C. Wicks, and R. D. Brown, "A deterministic least-squares approach to space-time adaptive processing (stap)," *IEEE Transactions on Antennas and Propagation*, vol. 49, no. 1, pp. 91–103, 2001.

[15] A. J. Weiss and A. Amar, "Direct position determination of multiple radio signals," *EURASIP Journal on Applied Signal Processing*, vol. 2005, pp. 37–49, Jan. 2005.

[16] A. Y. Sidi and A. J. Weiss, "Delay and doppler induced direct tracking by particle filter," *IEEE Transactions on Aerospace and Electronic Systems*, vol. 50, no. 1, pp. 559–572, 2014.

[17] N. Garcia, A. M. Haimovich, J. A. Dabin, M. Coulon, and M. Lops, "Direct localization of emitters using widely spaced sensors in multipath environments," pp. 695–700, 2014.

[18] S. Blackman, "On phased-array radar tracking and parameter control," *IEEE Transactions on aerospace and electronic systems*, vol. 29, no. 1, 1993.

[19] S. Blackman and R. Popoli, *Modern Tracking Systems*. Norwood, MA: Artech House, 1999.

[20] W. F. Leven and A. D. Lanterman, "Unscented kalman filters for multiple target tracking with symmetric measurement equations," *IEEE Transactions on Automatic Control*, vol. 54, no. 2, pp. 370–375, 2009.

[21] H. Godrich, V. M. Chiriac, A. M. Haimovich, and R. S. Blum, "Target tracking in mimo radar systems: Techniques and performance analysis," in *Radar Conference, 2010 IEEE*. IEEE, 2010, pp. 1111–1116.

[22] J. Ward, "Space-time adaptive processing for airborne radar," MIT Lincoln Laboratory, Lexington, MA, Tech. Rep. 1015, Dec. 1994.

[23] R. Klemm, "Principles of space-time adaptive processing," *No. 12. IET,*, vol. 12, no. 12, 2002.

[24] D. B. Leeson, "Oscillator phase noise: A 50-year retrospective," *2015 Joint Conference of the IEEE International Frequency Control Symposium & the European Frequency and Time Forum*, pp. 332–337, 2015.

[25] "Special issue on frequency stability," in *Proc IEEE*, vol. 54, no. 2, Feb., pp. 101–338.

[26] D. Allan, "Statistics of atomic frequency standards," *Proc. IEEE*, vol. 54, no. 2, pp. 221–230, Feb. 1966.

[27] D. B. Leeson, "A simple model of feedback oscillator noise spectrum," in *Proceedings of the IEEE*, vol. 54, no. 2, Feb. 1996, pp. 329–330.

[28] F. Walls and D. Allan, "Measurements of frequency stability," *Proceedings of the IEEE*, vol. 74, no. 1, pp. 162–168, 1986.

[29] "1139-2008 - ieee standard definitions of physical quantities for fundamental frequency and time metrology—random instabilities," in *IEEE*, Feb. 2009.

[30] W. J. Riley, "Handbook of stability analysis, nist publication 1065," *National Institute of Standards and Technology*, July 2008.

[31] G. Haslam and B. Reid, "Motion sensing requirements for synthetic aperture radar," *1983 lFFC Proc (Toronto, ON, Can)*, vol. 1, pp. 126–131, 1983.

[32] G. Krieger and M. Younis, "Impact of oscillator noise in bistatic and multistatic sar," *IEEE Geoscience and Remote Sensing Letters 3*, no. 3, pp. 424–428, 2006.

[33] D. B. Leeson, "A simple model of feedback oscillator noise spectrum," *Proceedings of the IEEE*, vol. 54, no. 2, pp. 329–330, Feb. 1966.

[34] A. Aubry, V. Carotenuto, A. De Maio, and A. Farina, "Radar phase noise modeling and effects-part ii: pulse doppler processors and sidelobe blankers," *IEEE Transactions on Aerospace and Electronic Systems*, vol. 52, no. 2, pp. 712–725, 2016.

[35] K. S. Ubolkosold, Pakorn and O. Loffeld, "Estimation of oscillators phase offset, frequency offset, and rate of change for bistatic interferometric sar," *Proceedings of European Conference on Synthetic Aperture Radar (EUSAR)*, vol. 300, April 2006.

[36] B. Friedlander and A. J. Weiss, "Eigenstructure methods for direction finding with sensor gain and phase uncertainties," pp. 2681–2684, 1988.

[37] B. P. Flanagan and K. L. Bell, "Array self-calibration with large sensor position errors," *Signal Processing*, vol. 81, no. 10, pp. 2201–2214, 2001.

[38] A. Liu, G. Liao, C. Zeng, Z. Yang, and Q. Xu, "An eigenstructure method for estimating doa and sensor gain-phase errors," *IEEE Transactions on signal processing*, vol. 59, no. 12, pp. 5944–5956, 2011.

[39] S. M. Kay, *Fundementals of Statistical Signal Processing: Estimation Theory.* New Jersey: Parentice Hall PTR, 1st ed., 1993.

[40] H. L. V. Trees, K. L. Bell, and Y. Wang, "Bayesian cramer-rao bounds for multistatic radar," in *2006 International Waveform Diversity Design Conference*, 2006, pp. 1–4.

[41] P. Tichavsky, C. H. Muravchik, and A. Nehorai, "Posterior cramér-rao bounds for discrete-time nonlinear filtering," *IEEE Transactions on signal processing*, vol. 46, no. 5, pp. 1386–1396, 1998.

[42] A. M. Demir, Alper and J. Roychowdhury, "Phase noise in oscillators: a unifying theory and numerical methods for characterization," *IEEE Transactions on Circuits and Systems I: Fundamental Theory and Applications*, vol. 47, no. 5, pp. 655–674, 2000.

[43] A. Demir, "Phase noise and timing jitter in oscillators with colored-noise sources," *IEEE Transactions on Circuits and Systems I: Fundamental Theory and Applications*, vol. 49, no. 12, pp. 1782–1791, Dec. 2002.

[44] G. W. J. Barnes, "Characterization of frequency stability," *IEEE Transactions on Instrumentation and Measurement*, no. 2, pp. 105–120, May. 1971.

[45] J. Vig, "Quartz crystal resonators and oscillators," *US Army Communications-Electronics Command*, Jan. 2004.

[46] J. R. Vig, C. Audoin, L. S. Cutler, M. M. Driscoll, and E. P. EerNisse, "The effects of acceleration on precision frequency sources," 1992.

[47] D. Allan, H. Hellwig, P. Kartaschoff, J. Vanier, J. Vig, G. M. Winkler, and N. Yannoni, "Standard terminology for fundamental frequency and time metrology," pp. 419–425, 1988.

[48] A. Chorti and M. Brookes, "A spectral model for rf oscillators with power-law phase noise," *IEEE Transactions on Circuits and Systems I: Regular Papers*, vol. 53, no. 9, pp. 1989–1999, Sept. 2006.

[49] C. A. Greenhall, "An approach to power-law phase-noise models through generalized functions," *Metrologia*, vol. 47, no. 5, p. 605, 2010.

[50] D. Petrovic, W. Rave, and G. Fettweis, "Effects of phase noise on ofdm systems with and without pll: Characterization and compensation," *IEEE Transactions on Communications*, vol. 55, no. 8, pp. 1607–1616, 2007.

[51] S. Wu, P. Liu, and Y. Bar-Ness, "Phase noise estimation and mitigation for ofdm systems," *IEEE Transactions on Wireless Communications*, vol. 5, no. 12, 2006.

[52] V. Syrjala, M. Valkama, N. N. Tchamov, and J. Rinne, "Phase noise modelling and mitigation techniques in ofdm communications systems," in *Wireless Telecommunications Symposium, 2009. WTS 2009.* IEEE, 2009, pp. 1–7.

[53] A. A. Nasir, H. Mehrpouyan, R. Schober, and Y. Hua, "Phase noise in mimo systems: Bayesian cramer–rao bounds and soft-input estimation," *IEEE Transactions on Signal Processing*, vol. 61, no. 10, pp. 2675–2692.

[54] W. A. LLC, "Multiplied crystal oscillator (mxo-plm) spreadsheet," in *http://www.Welzel.com/model/mxoplm/*, online accessed June 23rd, 20186.

[55] J. Auterman, "Phase stability requirements for a bistatic sar," Atlanta, USA, 1984, pp. 48–52.

[56] S. Buckreuss, "Motion errors in an airborne synthetic aperture radar system," *European Transactions on Telecommunications 2*, no. 6, pp. 655–664, 1991.

[57] D. Hounam and K. Wägel, "Oscillator noise and sar image quality," *DLR Res. Report*, 1994.

[58] Y. Gruson, V. Giordano, U. L. Rohde, A. K. Poddar, and E. Rubiola, "Cross-spectrum pm noise measurements, thermal energy, and metamaterial filters," *IEEE Transact. Ultrason., Ferroelec. Freq. Control*, vol. 64, no. 3, pp. 634–641, March 2017.

[59] J. Timmer and M. Koenig, "On generating power law noise." *Astronomy and Astrophysics*, vol. 300, p. 707, 1995.

[60] N. Ashby, "Confidence estimates in simulation of phase noise or spectral density," *IEEE Transactions on Ultrasonics, Ferroelectrics, and Frequency Control*, vol. 64, no. 5, pp. 872–878, May 2017.

[61] Y. Lo, "A mathematical theory of antenna arrays with randomly spaced elements," *IEEE Transactions on Antennas and Propagation*, vol. 12, no. 3, pp. 257–268, 1964.

[62] B. Steinberg, "The peak sidelobe of the phased array having randomly located elements," *IEEE Transactions on Antennas and Propagation*, vol. 20, no. 2, pp. 129–136, 1972.

[63] H. H. Kim and A. M. Haimovich, "Design of cfar radars using compressive sensing," *Proc. IEEE Radar Conf.*, pp. 1–6, May 2016.

[64] S. Coutts and K. Cuomo, "Distributed coherent aperture measurements for next generation bmd radar," in *Fourth IEEE Workshop on Sensor Array and Multichannel Processing, 2006.*, July 2006, pp. 390–393.

[65] O. Abari and H. Rahul, "Airshare: Distributed coherent transmission made seamless," in *2015 IEEE Conference on Computer Communications (INFOCOM)*, April 2015, pp. 1742–1750.

[66] D. R. Brown and U. Madhow, "Receiver-coordinated distributed transmit nullforming with channel state uncertainty," in *2012 46th Annual Conference on Information Sciences and Systems (CISS)*, March 2012, pp. 1–6.

[67] X. Yang, P. Yin, and T. Zeng, "Time and phase synchronization for wideband distributed coherent aperture radar," 2013.

[68] E. Lee and C. N. Dorny, "A broadcast reference technique for self-calibrating of large antenna phased arrays," *IEEE Transactions on Antennas and Propagation*, vol. 37, no. 8, pp. 1003–1010, Aug 1989.